Australia Cretaceous climate and tectonics

Huber, Brian T.; Hobbs, Richard W.; Bogus, Kara A.; Batenburg, Sietske J.; Brumsack, Hans Jürgen; Do Monte Guerra, Rodrigo; Edgar, Kirsty M.; Edvardsen, Trine; Harry, Dennis L.; Hasegawa, Takashi; Haynes, Shannon J.; Jiang, Tao; Jones, Matthew M.; Kuroda, Junichiro; Lee, Eun Young; Li, Yong Xiang; MacLeod, Kenneth G.; Maritati, Alessandro; Martinez, Mathieu; O'Connor, Lauren K.

DOI:
10.14379/iodp.pr.369.2018

International Ocean Discovery Program Expedition 369 Preliminary Report

Australia Cretaceous Climate and Tectonics

Tectonic, paleoclimate, and paleoceanographic history of high-latitude southern margins of Australia during the Cretaceous

26 September–26 November 2017

B.T. Huber, R.W. Hobbs, K.A. Bogus, and the Expedition 369 Scientists

IODP
INTERNATIONAL OCEAN DISCOVERY PROGRAM

Publisher's notes

Core samples and the wider set of data from the science program covered in this report are under moratorium and accessible only to Science Party members until 25 May 2019.

This publication was prepared by the *JOIDES Resolution* Science Operator (JRSO) at Texas A&M University (TAMU) as an account of work performed under the International Ocean Discovery Program (IODP). Funding for IODP is provided by the following international partners:

National Science Foundation (NSF), United States
Ministry of Education, Culture, Sports, Science and Technology (MEXT), Japan
European Consortium for Ocean Research Drilling (ECORD)
Ministry of Science and Technology (MOST), People's Republic of China
Korea Institute of Geoscience and Mineral Resources (KIGAM)
Australia-New Zealand IODP Consortium (ANZIC)
Ministry of Earth Sciences (MoES), India
Coordination for Improvement of Higher Education Personnel (CAPES), Brazil

Portions of this work may have been published in whole or in part in other IODP documents or publications.

Disclaimer

Any opinions, findings, and conclusions or recommendations expressed in this publication are those of the author(s) and do not necessarily reflect the views of the participating agencies, TAMU, or Texas A&M Research Foundation.

Copyright

Citation

Huber, B.T., Hobbs, R.W., Bogus, K.A., and the Expedition 369 Scientists, 2018. *Expedition 369 Preliminary Report: Australia Cretaceous Climate and Tectonics.* International Ocean Discovery Program. https://doi.org/10.14379/iodp.pr.369.2018

ISSN
World Wide Web: 2372-956

February 2018

Expedition 369 participants

Expedition 369 scientists

Brian T. Huber
Co-Chief Scientist
National Museum of Natural History
Smithsonian Institution
USA
huberb@si.edu

Richard W. Hobbs
Co-Chief Scientist
Department of Earth Sciences
University of Durham
United Kingdom
r.w.hobbs@durham.ac.uk

Kara A. Bogus
Expedition Project Manager/Staff Scientist
International Ocean Discovery Program
Texas A&M University
USA
bogus@iodp.tamu.edu

Sietske J. Batenburg
Stratigraphic Correlator
Department of Earth Sciences
University of Oxford
United Kingdom
sietske.batenburg@earth.ox.ac.uk

Hans-Jürgen Brumsack
Inorganic Geochemist
Institut für Chemie und Biologie des Meeres (ICBM)
Carl von Ossietzky Universität Oldenburg
Germany
brumsack@icbm.de

Rodrigo do Monte Guerra
Paleontologist (nannofossils)
Technological Institute of Micropaleontology
Universiadde do Vale do Rio dos Sinos (UNISINOS)
Brazil
rodrigomguerra1@gmail.com

Kirsty M. Edgar
Paleontologist (foraminifers)
School of Geography, Earth and Environmental Sciences
University of Birmingham
United Kingdom
k.m.edgar@bham.ac.uk

Trine Edvardsen
Paleontologist (benthic foraminifers)
Natural History Museum of Denmark
University of Copenhagen
Denmark
trine.arp@snm.ku.dk

Dennis L. Harry
Physical Properties Specialist
Department of Geosciences
Colorado State University
USA
dennis.harry@colostate.edu

Takashi Hasegawa
Organic Geochemist
Department of Earth Sciences
Faculty of Natural Systems
Kanazawa University
Japan
jh7ujr@staff.kanazawa-u.ac.jp

Shannon J. Haynes
Sedimentologist
Department of Geosciences
Princeton University
USA
sjhaynes@princeton.edu

Tao Jiang
Sedimentologist
College of Marine Science and Engineering
China University of Geosciences
China
taojiang@cug.edu.cn

Matthew M. Jones
Physical Properties Specialist/Downhole Measurements
Earth and Planetary Sciences
Northwestern University
USA
matthewjones2012@u.northwestern.edu

Junichiro Kuroda
Sedimentologist
Atmosphere and Ocean Research Institute
University of Tokyo
Japan
kuroda@aori.u-tokyo.ac.jp

Eun Young Lee
Physical Properties Specialist
Faculty of Earth Systems and Environmental Sciences
Chonnam National University
Republic of Korea
eun.y.leeee@gmail.com

Yong-Xiang Li
Paleomagnetist
School of Earth Sciences and Engineering
Nanjing University
China
yxli@nju.edu.cn

Kenneth G. MacLeod
Stratigraphic Correlator
Department of Geological Sciences
University of Missouri, Columbia
USA
macleodk@missouri.edu

Alessandro Maritati
Sedimentologist
Institute of Marine and Antarctic Studies (IMAS)
University of Tasmania
Australia
alessandro.maritati@utas.edu.au

Mathieu Martinez
Physical Properties Specialist
Geosciences Rennes
University of Rennes 1
France
Mathieu.martinez@univ-rennes1.fr

Lauren K. O'Connor
Organic Geochemist
Department of Earth Sciences
University of Oxford
United Kingdom
lauren.oconnor@univ.ox.ac.uk

Maria Rose Petrizzo
Paleontologist (foraminifers)
Department of Earth Sciences
Università degli Studi di Milano
Italy
mrose.petrizzo@unimi.it

Tracy M. Quan
Inorganic Geochemist
Boone Pickens School of Geology
Oklahoma State University
USA
tracy.quan@okstate.edu

Carl Richter
Paleomagnetist
School of Geosciences
University of Louisiana at Lafayette
USA
richter@louisiana.edu

Laurent Riquier
Sedimentologist
Institut des sciences de la Terre a Paris (ISTEP)
University Pierre et Marie Curie
France
laurent.riquier@upmc.fr

Gabriel T. Tagliaro
Sedimentologist
Institute for Geophysics
University of Texas at Austin
USA
gtagliaro@utexas.edu

Maria Luisa Garcia Tejada
Petrologist
Institute for Research on Earth Evolution (IFREE)
Japan Agency for Marine-Earth Science and Technology
Japan
mtejada@jamstec.go.jp

Carmine C. Wainman
Sedimentologist/Observer
Australian School of Petroleum
University of Adelaide
Australia
carmine.wainman@adelaide.edu.au

David K. Watkins
Paleontologist (nannofossils)
Earth and Atmospheric Sciences
University of Nebraska, Lincoln
USA
dwatkins1@unl.edu

Lloyd T. White
Physical Properties Specialist/Downhole Measurements
School of Earth and Environmental Sciences
University of Wollongong
Australia
lloydw@uow.edu.au

Erik Wolfgring
Paleontologist (benthic foraminifers)
Department of Geodynamics and Sedimentology
Department of Paleontology
University of Vienna
Austria
erik.wolfgring@univie.ac.at

Zhaokai Xu
Sedimentologist
Institute of Oceanology
Chinese Academy of Sciences
China
zhaokaixu@qdio.ac.cn

Education and outreach

Vivien Cumming
Education Officer
United Kingdom
viviencumming@gmail.com

Charissa Ruth
Education Officer
USA
charissa.ruth@gmail.com

Cristiane Delfina
Education Officer
Brazil
contactdelfina@gmail.com

Operational and technical staff

Siem Offshore AS officials

Terry Skinner
Master of the Drilling Vessel

Sam McLelland
Offshore Installation Manager

Technical support

Alexis Armstrong
X-ray Laboratory

Heather Barnes
Assistant Laboratory Officer

Etienne Claassen
Marine Instrumentation Specialist

William Crawford
Senior Imaging Specialist

Benjamin Daniel
Core Laboratory

Seth Frank
Thin Section Laboratory

Edwin Garrett
Paleomagnetics Laboratory

Rachael Gray
Core Laboratory

Margaret Hastedt
Assistant Laboratory Officer

Jennifer Hutchinson
Marine Computer Specialist

Jurie Kotze
Marine Instrumentation Specialist

Jurie Kotze, Jr.
Temporary Technician

Brittany Martinez
Curatorial Specialist

Zenon Mateo
Underway Geophysics Laboratory

Erik Moortgat
Chemistry Laboratory

Algie Morgan
Application Developer

Chieh Peng
Laboratory Officer

Vincent Percuoco
Chemistry Laboratory

Bill Rhinehart
Operations Superintendent

Catherine Smith
Temporary Technician

Alyssa Stephens
Publications Specialist

Kerry Swain
Logging Engineer

Steven Thomas
Marine Computer Specialist

Hai (James) Zhao
Applications Developer

Abstract

The tectonic and paleoceanographic setting of the Great Australian Bight (GAB) and the Mentelle Basin (MB; adjacent to Naturaliste Plateau) offered an outstanding opportunity to investigate Cretaceous and Cenozoic climate change and ocean dynamics during the last phase of breakup among remnant Gondwana continents. Sediment recovered from sites in both regions during International Ocean Discovery Program Expedition 369 will provide a new perspective on Earth's temperature variation at sub-polar latitudes (60°–62°S) across the extremes of the mid-Cretaceous hot greenhouse climate and the cooling that followed. The primary goals of the expedition were to

- Investigate the timing and causes for the rise and collapse of the Cretaceous hot greenhouse climate and how this climate mode affected the climate-ocean system and oceanic biota;
- Determine the relative roles of productivity, ocean temperature, and ocean circulation at high southern latitudes during Cretaceous oceanic anoxic events (OAEs);
- Identify the main source regions for deep-water and intermediate-water masses in the southeast Indian Ocean and how these changed during Gondwana breakup;
- Characterize how oceanographic conditions at the MB changed during the Cenozoic opening of the Tasman Passage and restriction of the Indonesian Gateway;
- Resolve questions on the volcanic and sedimentary origins of the Australo-Antarctic Gulf and Mentelle Basin and provide stratigraphic control on the age and nature of the prebreakup successions.

Hole U1512A in the GAB recovered a 691 m thick sequence of black claystone ranging from the early Turonian to the early Campanian. Age control is primarily based on calcareous nannofossils, but the presence of other microfossil groups provided consistent but low-resolution control. Despite the lithologic uniformity, long- and short-term variations in natural gamma ray and magnetic susceptibility intensities show cyclic alternations that suggest an orbital control of sediment deposition that will be useful for developing an astrochronology for the sequence.

Sites U1513–U1516 were drilled between 850 and 3900 m water depth in the MB and penetrated 774, 517, 517, and 542 meters below seafloor (mbsf), respectively. Under a thin layer of Pleistocene–upper Miocene sediment, Site U1513 cored a succession of Cretaceous units from the Campanian to the Valanginian. Site U1514 sampled an expanded Pleistocene–Eocene sequence and terminated in the upper Albian. The Cenomanian–Turonian interval at Site U1514 recovered deformed sedimentary rocks that probably represent a detachment zone. Site U1515 is located on the west Australian margin at 850 m water depth and was the most challenging site to core because much of the upper 350 m was either chert or poorly consolidated sand. However, the prebreakup Jurassic(?) sediments interpreted from the seismic profiles were successfully recovered. Site U1516 cored an expanded Pleistocene, Neogene, and Paleogene section and recovered a complete Cenomanian/Turonian boundary interval containing five layers with high total organic carbon content.

Recovery of well-preserved calcareous microfossil assemblages from different paleodepths will enable generation of paleotemperature and biotic records that span the rise and collapse of the Cretaceous hot greenhouse (including OAEs 1d and 2), providing insight to resultant changes in deep-water and surface water circulation that can be used to test predictions from earth system models. Paleotemperature proxies and other data will reveal the timing, magnitude, and duration of peak hothouse temperatures and any cold snaps that could have allowed growth of a polar ice sheet. The sites will also record the mid-Eocene–early Oligocene opening of the Tasman Gateway and the Miocene–Pliocene restriction of the Indonesian Gateway; both passages have important effects on global oceanography and climate. Understanding the paleoceanographic changes in a regional context provides a global test on models of Cenomanian–Turonian oceanographic and climatic evolution related both to extreme Turonian warmth and the evolution of OAE 2.

The Early Cretaceous volcanic rocks and underlying Jurassic(?) sediments cored in different parts of the MB provide information on the timing of different stages of the Gondwana breakup. The recovered cores provide sufficient new age constraints to underpin a reevaluation of the basin-wide seismic stratigraphy and tectonic models for the region.

Introduction

Understanding the mechanisms, feedbacks, and temporal relationships that link climate dynamics between the polar regions and the tropics is of fundamental importance for reconstructing rapid climate change in the past and hence improving predictions in the future. High-resolution stratigraphic records from strategic locations around the globe, especially from the high-latitude oceans, are essential to achieve this broader goal. Within this context, past periods of extreme warmth such as the Cretaceous hot greenhouse and the initial Eocene thermal maximum have attracted increasing research interest over recent years, resulting in often spectacular and sometimes contradictory insights into the mechanisms of natural short-term changes in climate, biogeochemical cycling, and ocean oxygenation. IODP Expedition 369 targeted these fundamental objectives with specific goals of providing high-latitude Southern Ocean sites with expanded late Mesozoic and Cenozoic sections and improving constraints on the tectonic history of the region.

Expedition 369 recovered sediments from the Great Australian Bight (GAB) and Mentelle Basin (MB) that will provide new insights to the evolution of Southern Hemisphere, high-latitude Cretaceous climates. The high paleolatitude (60°–62°S) location of the sites (Figure **F1**) is especially important for global climatic studies because of the enhanced sensitivity to changes in ocean temperature. Study of the recovered sections will enable generation of high-resolution stratigraphic records across the rise and collapse of the Cretaceous hot greenhouse climate and concomitant changes in Earth's latitudinal thermal gradients and deep ocean circulation that continued through the Cenozoic. The well-resolved age framework of the pelagic carbonate sequences will enable more precise correlation between global climatic shifts and tectonic history, especially major volcanic episodes in the region. These aspects are crucial to improve our understanding of Earth's climate system and to inform the scientific modeling community on high-latitude Southern Hemisphere Cretaceous (and possibly older) records in a currently underexplored region.

Background

Geological setting

Following the collision of Gondwana with Laurasia at 330–320 Ma, which formed the supercontinent of Pangaea, the breakup of

eastern Gondwana commenced during the Jurassic (Veevers, 2006). At this time, the Naturaliste Plateau (NP) was located near the triple junction of the Australian, Antarctic, and Greater India plates (Figure **F1**) at 60°–62°S. The first stage of breakup occurred as India separated from Australia. Later, in the early Eocene, Australia separated from Antarctica.

The Mentelle Basin and rifting of Greater India

The MB separates the NP from western Australia and is part of a sequence of basins along the western margin of Australia that formed during the breakup with India (Bradshaw et al., 2003). The rifting episode initiated in northwestern Australia in what is now the Argo Abyssal Plain and then propagated southward in a series of en echelon basins with the MB being the furthest south (Maloney et al., 2011). The MB is separated from the Perth Basin by the basement high of the Leeuwin Block and the Yallingup Shelf (Figure **F2**). Despite its water depth (2000–4000 m), the basement under the MB is believed to be continental. The MB is believed to contain Jurassic and possibly older sediments that were deposited in syn- and post-rift basins. During the breakup with Greater India, the NP is classed as part of a volcanic margin as evidenced by the onshore Bunbury basalt, which recent dating has given an age of 137–130 Ma. This date is contemporaneous with the final stages of rifting but older than the basalt found on the Kerguelen Plateau, even though the geochemistry is similar (Olierook et al., 2016). Basalt is widely dredged around the NP and, as has been documented on volcanic margins elsewhere (Planke et al., 1999), is the cause of the strong seismic reflection echo seen on seismic profiles that cross the MB and denote the top of the Valaginian. Younger sediments were deposited in a thermally subsiding basin and margin. Deep Sea Drilling Project (DSDP) Site 258 previously drilled this post-rift section on the western margin of the MB but stopped short of the interpreted basalt horizon.

Seismic data acquired in 2004 and 2009 by Geoscience Australia (tied to Site 258) provided a regional survey to appraise the stratigraphic, structural, and depositional history of the MB (Maloney et al., 2011; Borissova et al., 2010). Relatively young Neogene carbonate oozes unconformably overlie Paleogene deep marine chalk. Occasional bright reflection events in this sequence are likely caused by thin chert bands. This Paleogene chalk unconformably overlies Cretaceous coccolith-rich chalk that is underlain by Albian/Aptian claystones that pinch out against a glauconitic sandstone. The unconformity at the base of the ooze and the top of the glauconitic sandstone can be identified and interpreted from the seismic data; the other boundaries do not create distinct reflections. The glauconitic sandstone sequence is floored by a high-amplitude reflection (not sampled at Site 258) that is interpreted to be caused by Valanginian volcanics. Hence, this horizon coincides with the onset of breakup and separation of Greater India from Australia and a series of subsequent volcanic episodes related to the continuing breakup on the northern and western margins of the NP. Prior rifting of the area is recorded by Early Cretaceous, Jurassic, and Permian/Triassic sequences, although the interpretation is somewhat speculative because the sequences lacked borehole control.

Opening of the Australo-Antarctic Gulf

The breakup on the southern margin of Australia is thought to have started in the Cenomanian–Turonian (Direen et al., 2011) and proceeded at a very slow rate. Contrary to the rifting of Greater India, this margin is believed to be nonvolcanic, but plate tectonic reconstructions corresponding to these early stages of rifting are poorly constrained and controversial (White et al., 2013). The ~15 km thick post-Middle Jurassic sedimentary sequence that accumulated in the GAB contains the largest continental margin deltaic sequence deposited during the Late Cretaceous greenhouse. Accelerated subsidence commencing in the late Albian and continuing through the Cenomanian–Santonian led to the deposition of a thick sequence of marine shales (Totterdell et al., 2000). During the Cretaceous, the GAB was situated at the eastern tip of a partial seaway, the Australo-Antarctic Gulf (AAG), with the NP in the open ocean at the western gateway that connected the AAG with the southern Indian Ocean.

An overall transgressive phase of sedimentation in the early Paleogene was followed by the establishment of open marine carbonate shelf conditions from the early Eocene onward. The AAG eventually widened to create the Southern Ocean with a switch to rapid spreading after 45 Ma (White et al., 2013). An industry well, Jerboa-1, in the Eyre subbasin on the continental shelf provided a stratigraphic tie along seismic profile AGSO Survey 65 Line 06 (Bradshaw et al., 2003).

Opening of the Indian Ocean and Tasman Gateway and closure of the Indonesian Gateway

After initial rifting, India drifted in a north-northwest direction with strike-slip motion along the Wallaby-Zenith Fracture Zone. This juxtaposed their continental shelves until ~120 Ma, isolating the nascent Indian Ocean from global deep-water circulation (Gibbons et al., 2013). Subsequently, the northward drift of Australia through the Cenozoic affected changes in two important ocean gateways to the Indian Ocean: the opening of the Tasman Gateway between Australia and Antarctica in the middle Eocene–early Oligocene and the restriction of the Indonesian Gateway between Australia and Southeast Asia in the Miocene–Pliocene. Both passages have important effects on global oceanography and climate, and the NP/MB region is well situated to monitor their opening history and resultant effects on ocean circulation (Figure **F3**).

The Antarctic Circumpolar Current (ACC) in the Southern Ocean is central to the present-day overturning circulation and surface heat redistribution (Lumpkin and Speer, 2007). Although there is no significant restriction on the ACC in the modern Tasman Passage, the Tasman and Drake Passages both opened during the middle Eocene–Oligocene, and the restriction to flow at the Tasman Passage would have been significant for ocean circulation, especially in the late Eocene–early Oligocene. During the Paleocene–Eocene, southern Australia would have been influenced more by subpolar (rather than the modern subtropical) gyres as a consequence of the closed or restricted Tasman Passage and more southerly position of Australia (e.g., Huber et al., 2004). During the Early Eocene Climatic Optimum, however, temperatures in the southwest Pacific Ocean near Australia seem to have been warmer than climate models predict (Hollis et al., 2012). Cooling of the Antarctic margin relative to the Australian margin near Tasmania occurred early in the opening of the Tasman Passage, which is dated at 49–50 Ma (Bijl et al., 2013), and differentiation of deepwater produced in the Southern Ocean relative to the North Atlantic began in the late middle Eocene (Cramer et al., 2009; Borrelli et al., 2014). However, plate tectonic reconstructions (Müller et al., 2000) indicate that separation of Australia and Antarctica near Tasmania occurred later (~43 Ma). Recovering material spanning this time interval thus provides an important opportunity to reconcile these tectonic and paleoceanographic interpretations.

The restricted surface flow through the Indonesian Gateway is essential to the surface heat flux in the Pacific and Indian Oceans and has been linked to El Niño Southern Oscillation (ENSO) dynamics and the global ocean overturning circulation (Gordon, 1986; Godfrey, 1996; Lee et al., 2002). The gradual restriction of the Indonesian Passage from deep-water throughflow in the late Oligocene–early Miocene to variable shallow flow in the Pliocene–Pleistocene is thought to have strongly affected surface heat distribution with potential links to the late Neogene cooling and Northern Hemisphere glaciation (Cane and Molnar, 2001; Kuhnt et al., 2004; Karas et al., 2009).

Objectives

1. *Investigate the timing and causes for the rise and collapse of the Cretaceous hot greenhouse and how this climate mode affected the climate-ocean system and oceanic biota.*

Compilations of deep-sea benthic foraminiferal and bulk carbonate $\delta^{18}O$ data reveal that the world ocean experienced long-term warming from the late Aptian through middle Cenomanian, maintained extremely warm temperatures from the late Cenomanian through Santonian with peak warmth during the Turonian (>20°C at midbathyal depths), and gradually returned to cooler values (~6°–8°C at midbathyal depths) during the Maastrichtian (Huber et al., 1995, 2002, 2011; Clarke and Jenkyns, 1999; Friedrich et al., 2012; O'Brien et al., 2017). Recent benthic and planktonic $\delta^{18}O$ values obtained from the Turonian at Site 258 support extreme high-latitude Turonian warmth (Huber et al., submitted). Still, these $\delta^{18}O$ values are problematically low and seem to defy straightforward explanations (Bice et al., 2003). These new analyses compared to existing stable isotope data (Huber et al., 1995, 2002) showed large changes at times of known climatic shifts. Relative to low-latitude sites, high-latitude sites are both undersampled and respond more strongly to climate change.

Although the Cretaceous has long been characterized as too warm to sustain continental ice sheets (e.g., Barron, 1983; Frakes et al., 1992; Huber et al., 2002; Hay, 2008), coincidences between sea level variations (deduced from sequence stratigraphy) and $\delta^{18}O$ records have been proposed by some authors as evidence for the occasional existence of polar ice (e.g., Barrera et al., 1997; Miller et al., 1999, 2005; Stoll and Schrag, 2000; Gale et al., 2002; Bornemann et al., 2008) and winter sea ice (Bowman et al., 2012). The "greenhouse glaciers" hypothesis has been countered by evidence for diagenetic influence on bulk carbonate oxygen isotope records and stable tropical planktonic and benthic foraminiferal δ18O data across several of the proposed cooling intervals (Huber et al., 2002; Moriya et al., 2007; Ando et al., 2009; MacLeod et al., 2013), Furthermore, TEX86 values from DSDP Site 511 suggest sea-surface temperatures during the Hauterivian–Aptian interval of 25°–30°C (Jenkyns et al., 2012; O'Brien et al., 2017).

High-resolution isotopic studies of samples from Expedition 369 sites should advance our understanding and improve geographic documentation of major global climatic warming and cooling transitions during the Cretaceous. Recovery of more complete sections will lead to biostratigraphic refinements and improved regional to global correlations.

2. *Determine the relative roles of productivity, ocean temperature, and ocean circulation at high southern latitudes during Cretaceous oceanic anoxic events (OAEs).*

OAEs are defined as short-lived (<1 My) episodes of enhanced deposition of organic carbon in a wide range of marine environments (Schlanger and Jenkyns, 1976) and are associated with prominent carbon isotope excursions in marine and terrestrial sequences (Jenkyns, 1980, 2010; Arthur et al., 1988; Gröcke et al., 1999; Jahren et al., 2001; Ando et al., 2002; Jarvis et al., 2006). Generation of OAEs has been attributed to a rapid influx of volcanogenic and/or methanogenic CO_2 sources leading to abrupt temperature rise and an accelerated hydrological cycle, increased continental weathering and nutrient discharge to oceans and lakes, intensified upwelling, and an increase in organic productivity. Globally expressed Cretaceous OAEs occurred during the early Aptian (OAE 1a; ~120 Ma) and at the Cenomanian/Turonian (C/T) boundary (OAE 2; ~94 Ma), whereas regionally recognized events occurred during the early Albian (OAE 1b; ~111 Ma) and late Albian (OAE 1d; ~100 Ma).

Cretaceous OAEs are best known from the Atlantic/Tethyan basins and surrounding continents, whereas Indian Ocean records are limited. The presence of black shales with as much as 6.9% total organic carbon (TOC) in the GAB (Totterdell et al., 2008), 11% at Site U1513 and up to 14% at Site U1516, suggest water may even have been euxinic in the region during deposition of OAE 2. OAE deposits should have been present at Kerguelen (Ocean Drilling Program [ODP] Site 1138) and Exmouth Plateaus and adjacent basinal areas (primarily ODP Site 763), but drilling strategies and poor recovery resulted in all of the cores missing the OAE record.

Recovery of a continuous record of the C/T boundary OAE 2 was anticipated at GAB Site U1512, western MB Site U1513, and northern MB Site U1514, although the actual recovery at Expedition 369 sites was different (see **Principal results**). At all sites, the anticipated OAE 2 interval is at a shallow burial depth (~260–460 meters below seafloor [mbsf]) where sediments are thermally immature and biogenic preservation is good to excellent. Observations and data will compare the Expedition 369 sites and other high-latitude OAE 2 sites to establish (1) whether significant changes in ocean circulation were coincident with OAE 2, (2) over what depth ranges (Zheng et al., 2013), and (3) whether OAE 2 in the high-latitude Southern Hemisphere was coincident with major changes in sea-surface temperatures (Jarvis et al., 2006). We were particularly interested in establishing whether the C/T succession contained evidence for the "Plenus cold event," an important cooling (~4 to >5°C) event within OAE 2 known from the Northern Hemisphere. This event is associated with changes in surface water circulation (e.g., Zheng et al., 2013) and reoxygenation of bottom water, but it remains unclear whether the Plenus cold event was a global or regional phenomenon. Data from the high southern latitudes are currently lacking (Jenkyns et al., 2012) and would address this critical gap in our model for OAE 2.

3. *Identify the main source regions for deep- and intermediate water masses in the southeast Indian Ocean and how these changed during the Gondwana breakup.*

Over the past few years, study of Cretaceous intermediate and deep-water circulation patterns has been galvanized by an increase

in published neodymium (Nd) isotopic data (e.g., Jiménez Berrocoso et al., 2010; Robinson et al., 2010; MacLeod et al., 2011; Martin et al., 2012; Murphy and Thomas, 2012; Jung et al., 2013; Moiroud et al., 2013; Voigt et al., 2013; Zheng et al., 2013). Nd isotopic values (expressed as εNd) have emerged as a promising proxy for reconstructing past circulation and are applicable across a wide range of water depths, including abyssal samples deposited below the carbonate compensation depth.

Typically measured on either phosphatic fossils (fish teeth, bones, and scales) or oxides leached from bulk samples, εNd values record a depositional to early diagenetic bottom water signature generally resistant to later diagenetic overprinting (Martin and Scher, 2004). The bottom water signature, in turn, reflects the εNd value of the source region of that water mass because Nd enters the ocean largely as riverine or eolian input, has a residence time shorter than the mixing time of the oceans, and has semiconservative behavior. Because εNd values in likely source regions vary by 10–15 units compared to an analytical precision of ~0.3 units, stratigraphic trends in εNd can be used to infer changes in circulation and mixing patterns through time. However, εNd values of samples are also influenced by local and global volcanic inputs, and the bottom water εNd signature of a water mass can be modified during circulation due to a high particle flux or boundary exchange, especially near detrital sources.

Cretaceous εNd data have been used to test, refine, and revise earlier circulation hypotheses that were based largely on carbon and oxygen isotopes. They have also documented correlation between εNd shifts and both long-term climate trends and shorter bioevents (e.g., OAE 2) and demonstrated a degree of complexity within and among sites not predicted by early studies. The latter is particularly true for the Southern Ocean, where circulation changes, water column stratification changes, volcanic inputs, and establishment of a widespread source of Southern Component Water have all been invoked to explain observed patterns (e.g., Robinson and Vance, 2012; Murphy and Thomas, 2012; Jung et al., 2013; Voigt et al., 2013). Neodymium studies of samples from sites representing a range of depths within the MB/NP, when combined with parallel paleotemperature estimates from $\delta^{18}O$ and TEX_{86} and documentation of calcareous microfossil assemblages, should help reduce uncertainty in interpretation of previous studies.

4. *Characterize how oceanographic conditions changed at the MB during the Cenozoic opening of the Tasman Passage and restriction of the Indonesian Gateway.*

The MB sites are well positioned to monitor paleoceanographic variations in the Leeuwin Current/Undercurrent system. The surface Leeuwin Current is unique in flowing poleward along the eastern boundary of the Indian Ocean (Figure **F3**). It is caused by the north–south gradient between cooler waters to the south and warm surface waters along the northwestern Australian coast. These warmer waters are derived from the Indonesian Throughflow (ITF) that overrides the prevailing wind stress and results in the poleward flow (Pattiaratchi, 2006; Godfrey, 1996; Domingues et al., 2007; Waite et al., 2007). The strength of the Leeuwin Current varies seasonally with the ITF strength and interannually with ENSO dynamics, strengthening in winter and under La Niña conditions. The intermediate Leeuwin Undercurrent is derived from an eddy system associated with the Flinders Current near the NP (Middleton and Cirano, 2002; Waite et al., 2007; Meuleners et al., 2007; Divakaran and Brassington, 2011). The Flinders Current and Leeuwin Undercurrent are conduits of the Tasman leakage, a pathway for return flow to the North Atlantic Ocean of deepwater upwelled in the Pacific and a component of the Southern Hemisphere super-gyre that links the subtropical gyres of the Atlantic, Pacific, and Indian Oceans (Speich et al., 2002, 2007; Ridgway and Dunn, 2007; van Sebille et al., 2012). The Tasman leakage allows interconnection of Antarctic Intermediate Water (AAIW) in the Pacific, Atlantic, and Indian Oceans, and the Flinders Current–Leeuwin Undercurrent system seems to play a role in the conversion of Subantarctic Mode Water to AAIW (Ridgway and Dunn, 2007). Deepwater in the MB is derived from Antarctic Bottom Water (AABW) and lower Circumpolar Deep Water that enter the Perth Basin between the MB and Broken Ridge, with substantial upwelling of AABW in the southern portion of the Perth Basin (Sloyan, 2006; McCartney and Donohue, 2007).

Coring in the MB complements previous drilling around Australia, especially off northwest and western Australia (DSDP Leg 27, ODP Legs 122 and 123, and International Ocean Discovery Program [IODP] Expedition 356) and southern Australia and Tasmania (ODP Legs 182 and 189). Coring recovered Paleocene–Eocene and upper Miocene–recent sequences at deep-water and intermediate water locations. Recovered material from this expedition will contribute to investigations of (1) the early Paleogene greenhouse climate at a high-latitude (~60°S) site, (2) oceanographic changes in the early stages of the opening of the Tasman Passage, and (3) oceanographic changes during the late stages of restriction of the Indonesian Passage.

5. *Resolve questions about the volcanic and sedimentary origins of the basin and provide stratigraphic control on the age and nature of the prebreakup succession.*

The interlinked aspects of the geology and evolution of the NP and MB suggest that recovering the volcanic rocks at the Valanginian/late Hauterivian unconformity will further our understanding of this region. Drilling the unconformity provides information on

1. The timing and position of the breakup (both on the western and southern margin, using paleomagnetic studies and $^{40}Ar/^{39}Ar$ dating of lavas),
2. The nature of the various phases of volcanism (core description, petrophysics, and geochemical and isotopic study),
3. Geographic and environmental reconstructions, and
4. The depositional history of the basin.

The principal cause of high-amplitude discontinuous reflectors overlying the Valanginian breakup unconformity corresponds to extrusive volcanics that flowed into the MB at the time of the breakup with Greater India. Drilling into the Valanginian volcanics and pre-Valanginian sediments (Sites U1513 and U1515) will provide stratigraphic control on the age and nature of the prebreakup succession and early rifting in the MB. Dating and analysis of the post-breakup sediments will provide needed information as to the development of the MB and particularly the influence of the later rifting with Antarctica. The results from this expedition will address a number of key tectonics questions for the region.

Principal results

Site U1512

Site background and objectives

The objective for coring Site U1512 (34°1.6407′S, 127°57.7604′E) was to obtain a continuous Upper Cretaceous record of marine black shales in the GAB across OAE 2, which strad-

dles the C/T boundary. Our plan was to compare the Site U1512 sediment record with coeval Expedition 369 sequences cored in the MB to characterize the geochemical and biological responses to extreme global carbon cycle perturbations in different paleoceanographic settings at high southern latitudes. Site U1512 lies in the GAB in ~3000 m of water on the continental slope. During the Cretaceous, the GAB was situated at the eastern tip of a partial seaway (the AAG), with the MB and NP in the open ocean at the western gateway that connected the AAG with the southern Indian Ocean. Studies of the recovered sequence of early Turonian–late Santonian marine claystone will provide new insight into the evolution of Late Cretaceous climate and oceanography in the region of the AAG.

Lithostratigraphy

The sedimentary sequence of Hole U1512A is divided into two main lithostratigraphic units (Figure **F4**). Unit I is a 10.06 m thick sequence of Pleistocene pinkish to white calcareous ooze with sponge spicules. The unit extends from the beginning of the hole to 10.06 m core depth below seafloor (CSF-A) (Sections 369-U1512A-1R-1 through 2R-1; 0–10.2 m CSF-A). The unit consists of medium and thick beds with no distinctive sedimentary structures, exhibits no bioturbation, and is massive and structureless. In this unit, biogenic grains are the major constituent and comprise dominant calcareous nannofossils, abundant foraminifers, and common sponge spicules. Unit II is a 690.32 m thick sequence of silty clay that gradationally transitions into silty claystone (Sections 2R-1 through 73R-CC at the bottom of the hole; 10.2–701.4 m CSF-A). This unit is black to dark gray mottled silty claystone composed of quartz, clay minerals, pyrite, siderite, and dolomite with varying degrees of bioturbation. Micropaleontological analysis indicates a Late Cretaceous (Santonian to Turonian) age for this unit. Lithostratigraphic Unit II is further divided into Subunits IIa (silty clay) and IIb (silty claystone) based on the degree of sediment lithification. Subunit IIa is 75.10 m thick and composed of very dark greenish gray to black unlithified silty clay. This subunit is characterized by the presence of pyrite both as nodules and in a disseminated form within the silty clay. Zeolite, foraminifers, calcareous nannofossils, and sponge spicules are present in trace amounts throughout the subunit. Inoceramid bivalve fragments and alteration halos occur frequently throughout the subunit. Subunit IIb is 615.22 m thick and is composed of lithified black silty claystone. Included in this subunit are 23 thin to medium beds of glauconitic and sideritic sandstone that are no thicker than 32 cm and mostly massive with normal grading. Bioclast traces present in this subunit include foraminifers, calcareous nannofossils, radiolarians, sponge spicules, and organic matter.

Biostratigraphy and micropaleontology

Samples from all Hole U1512A core catchers were analyzed for calcareous nannofossils, planktonic foraminifers, and benthic foraminifers. In addition, calcareous nannofossil assemblages were evaluated from split core sections. Observations of other distinctive and potentially age or environmentally diagnostic microfossil groups, such as organic-walled dinoflagellate cysts (dinocysts), radiolarians, fish debris, and inoceramid prisms, were also made in all core catcher samples. Calcareous nannofossil datums form the chronologic framework for Hole U1512A because they are most consistently present. In contrast, planktonic foraminifers are rare but, where present, have ages consistent with those from calcareous nannofossils. Similarly, rare dinocyst taxa from Cores 369-U1512A-47R through 70R (~440–672 m CSF-A) and radiolarians from Cores 5R through 35R (~38–333 m CSF-A) provide valuable additional age confirmation of Late Cretaceous sediments.

Core 1R is in calcareous nannofossil Zone CN15 and planktonic foraminiferal Subzone Pt1b and is upper Pleistocene/Holocene. Cores 2R through 4R are barren of calcareous nannofossils but contain rare planktonic foraminifers of both Cenozoic and Cretaceous species, which together with mixed radiolarian assemblage ages indicate downhole contamination during coring. Cores 5R and 6R are upper Santonian and lowermost Campanian calcareous nannofossil Zone CC17. Cores 7R through 11R (~57–104 m CSF-A) are assigned to latest Coniacian–Campanian calcareous nannofossil Zones CC16 and CC17. Cores 12R through 16R (~105–154 m CSF-A) are in Zone CC15, spanning the uppermost Coniacian and lowermost Santonian. Cores 17R through 20R (~154–192 m CSF-A) are Zone CC14 of Coniacian age. Cores 21R through 30R are mostly barren of all age diagnostic carbonate microfossils but likely span the C/T boundary. Cores 31R through 73R (to the base of the hole at 701.38 m CSF-A) are Turonian based on calcareous nannofossils in Cores 31R through 48R spanning Zone CC12, Cores 49R through 73R in Zone CC11, and Cores 65R through 73R in Zone CC10c.

Tubular agglutinated forms dominate benthic foraminiferal assemblages at Site U1512 and indicate either a lower to midbathyal environment or a marginal/restricted environment throughout the Late Cretaceous.

Paleomagnetism

The natural remanent magnetization (NRM) of all archive-half core sections and 21 discrete samples collected from the working halves of Hole U1512A were measured. The archive halves were stepwise treated with up to 30 mT alternating field (AF) demagnetization and measured with the pass-through superconducting rock magnetometer (SRM) at 5 cm intervals. The NRM intensity of the section is relatively weak and varies from 1.5×10^{-5} to 7.8×10^{-2} A/m with a mean of 5.5×10^{-4} A/m. The drilling-induced magnetic overprints can generally be removed by AF demagnetization at 10–20 mT. Inclinations of the characteristic remanent magnetizations (ChRMs) are predominantly negative, ranging from around −70° to −20°, indicating predominantly normal polarity. The uppermost ~80 m display a very noisy signal because of the significant coring disturbance (biscuiting) introduced by the rotary coring process. Positive inclination values occur between 0 and 75, 175 and 190, and 256 and 259 m CSF-A. The intervals from ~0 to 75 and 175 to 100 m CSF-A also exhibit sporadic or consecutive negative ChRM inclinations mixed with dominantly positive inclinations, making it impossible to assign magnetic polarity. The interval between 256 and 259 m CSF-A exhibits consistent downward-pointing paleomagnetic inclinations, defining a zone of reversed polarity that is probably associated with a short geomagnetic excursion.

Shipboard micropaleontological studies suggest that Core 5R (38.4–47.4 m CSF-A) is Santonian and the base of Core 73R is early Turonian. Therefore, the majority of the sedimentary cores from 38.4 to 700 m CSF-A document the uppermost segment of the 41.5 My Cretaceous normal Superchron C34n.

Petrophysics

Physical property data were obtained with the Whole-Round Multisensor Logger (WRMSL), Natural Gamma Radiation Logger (NGRL), *P*-wave velocity caliper (PWC), Section Half Multisensor Logger (SHMSL), and discrete samples. WRMSL *P*-wave measurements were discontinued deeper than Core 11R because of poor

contact between the core sections, their liners, and the caliper. NGR values (Figure **F4**) average 32.8 counts/s, and bulk density estimates from gamma ray attenuation (GRA) average 1.7 g/cm^3. GRA bulk density values in siltstone/claystone do not exceed 2.2 g/cm^3, whereas in siderite nodules and glauconitic sandstones they increase to 3.28 g/cm^3. WRMSL magnetic susceptibility values average 9.35 instrument units (IU), do not exceed 16 IU in claystone and siltstone, but increase to 253.58 IU in glauconitic sandstone and siderite; point measurements from the SHMSL agree with the trends. At scales longer than 10 m, the NGR and magnetic susceptibility records do not correlate over silty/clayey intervals from Cores 3R through 15R, possibly because of the high abundance of pyrite differentially influencing the magnetic susceptibility values. The NGR and GRA records display parallel trends in this interval. From Core 16R to 62R, pyrite abundance markedly decreases, and all three data types (magnetic susceptibility, NGR, and GRA density) display similar trends. From Core 63R to 73R, both NGR and magnetic susceptibility decrease, but GRA density remains stable. At shorter scales (<10 m), magnetic susceptibility, GRA density, and NGR show high-amplitude cycles of 3–5 m thickness in Cores 10R through 19R, 34R through 43R, and 62R through 73R. The range of *P*-wave velocities in the silty claystone range from 1670 to 2346 m/s, although faster velocities (3397–5774 m/s) were obtained for the discrete layers of sideritic sandstone. High-resolution (2 cm) reflectance spectroscopy and colorimetry data from archive-half core sections display high-amplitude variability.

On average, three discrete moisture and density (MAD) samples were taken from each core. Overall, the MAD results show that bulk density increases and grain density and porosity decrease. Bulk density for the dark silty claystone is 1.54–2.37 g/cm^3, and the density of the sideritic sandstone intervals ranges from 3.21 to 3.49 g/cm^3. Porosities in the silty claystone are 28%–65%, with most measurements between 40% and 48%. The porosity of the sideritic sandstone ranges from 5% to 13%.

Potassium (K), uranium (U), and thorium (Th) content were deconvolved from the NGR data. U/Th ratios are <0.2 throughout the entire hole, indicating oxic conditions during deposition. K/Th ratios sharply decrease in the uppermost 100 m, possibly caused by the presence of salt in this interval, which may increase the K content.

One downhole logging run measured NGR, density, sonic velocity, and resistivity values of the borehole wall using the triple combination (triple combo) tool string with the Dipole Shear Sonic Imager (modified triple combo tool string hereafter). Excellent borehole stability and favorable low-heave weather conditions permitted logging of the entire open borehole. Inclinometer readings progressively increase from roughly 0° shallower than 210 m wireline log matched depth below seafloor (WMSF) to 27° near the base of the hole, indicating that the borehole orientation deviated from vertical during coring. Background trends in density, NGR, and resistivity logs are relatively stable in the upper 300 m of the borehole. Below that interval, each of those three logs records minimum values near 325 m WMSF and then increases downhole to plateaus approaching maxima for the hole. Additionally, the density and resistivity logs preserve thin spikes in values that likely correspond to the thin sideritic and glauconitic sandstone beds commonly observed (see **Lithostratigraphy**). In general, downhole measurements record trends that are similar to those observed in the physical properties measured from the cores, such as meter-scale cyclicity in NGR (Figure **F4**), and provide a continuous petrophysical stratigraphy to span occasional gaps in core recovery.

Geochemistry

The geochemistry program was designed to characterize the composition of interstitial water and bulk sediments and to assess the potential presence of volatile hydrocarbons for routine safety monitoring. A total of 73 headspace gas samples were taken, and hydrocarbons were detected in 69 samples, although Cores 1R through 9R were broadly free of interstitial gas. Methane was the dominant gas detected (as high as 104,000 ppmv), with very minor ethane and occasional propane (up to 653 and 148 ppmv, respectively). Methane:ethane ratios suggest a transition from biogenic production above ~473 m CSF-A to possible thermogenic sources below that depth.

For interstitial water analyses, 46 samples were recovered from whole-round squeezing of sediment intervals. As a result of sediment lithology, interstitial water yield was low for the majority of the cores deeper than Core 12R (~115 m CSF-A). The final interstitial water sample was taken from Core 59R (~560 m CSF-A). The salinity of interstitial water samples generally decreases with depth due to decreases in sulfate (SO_4^{2-}), magnesium (Mg), and potassium (K) concentrations and general decreases in sodium (Na), bromide (Br^-), and chloride (Cl^-), possibly caused by low-salinity water present at greater depths. The dissolved Mg, K, and boron (B) concentration profiles reflect alteration of volcanic material and clay mineral formation. Sulfate is readily depleted within the upper ~93 m (Core 10R) of the sedimentary column (Figure **F4**) due to intense bacterial SO_4^{2-} reduction, which is accompanied by synchronous increases in ammonium (NH_4^+), alkalinity, and lithium (Li), along with high barium (Ba) values when SO_4^{2-} is exhausted. Alkalinity ranges from 4.4 to 16.52 mM with a maximum at 93.55 m CSF-A, and pH ranges from 7.76 to 7.97 with a slight decrease downhole; both measurements are limited to the uppermost ~130 m because of the small interstitial water volumes obtained from deeper samples. The dissolved calcium (Ca) and, to a lesser degree, strontium (Sr) concentration profiles show increasing concentrations toward 300 m CSF-A that are more than likely due to carbonate diagenesis. Decreasing Ca and Sr concentrations deeper than 300 m CSF-A indicate that carbonate dissolution/recrystallization may prevail at depth. Dissolved silicon (Si) shows a short positive excursion between 310.68 and 329.27 m CSF-A (Figure **F4**), reflecting the presence of biogenic opal-A in the sediment; lower values deeper than Core 35R may be due to opal-A/cristobalite and tridymite (CT) transformation. Elevated manganese (Mn) concentrations demonstrate the reducing character of the entire sedimentary sequence.

$CaCO_3$ content from Cores 1R through 73R varies from 0.06 to 6.66 wt% with the exception of Core 1R, which is composed of calcareous ooze with 90.97% $CaCO_3$. The low carbonate percentages in Cores 2R through 73R reflect the very low contribution of calcareous nannofossil and foraminiferal components to the sediment. TOC, which is predominantly terrestrially derived, ranges from 0.20 to 1.31 wt%, and total nitrogen (TN) ranges from <0.01 to 0.10 wt%. TOC/TN ratios generally decrease with depth, ranging from 6.30 to 31.19. This trend is likely caused by decomposition of nitrogen-containing terrestrial organic matter that released carbon as methane but retained the produced NH_4^+ in clays. Eight freeze-dried bulk sediment samples with TOC > 1 wt% were analyzed on the source rock analyzer. The results show very low hydrogen index values, and

the kerogen in the samples was classified as Type III, suggesting a predominantly terrestrial origin for the organic carbon.

Stratigraphic correlation

Only one hole was drilled at Site U1512 with the rotary core barrel (RCB) system. Recovery was excellent, exceeding 100% in 24 of the 73 cores recovered, and total recovery was 90%. Distinctive features for correlation included large-scale (>10 m) trends and changes of variable amplitude on shorter length scales (1–5 m) in NGR and magnetic susceptibility data, as well as distinct peaks corresponding to sandstone layers. Despite being unable to correlate cored intervals, recognition of matching features in NGR records from the Hole U1512A cores and wireline logs permitted a correlation of core depth scales from the CSF-A scale to the WMSF scale.

Age-depth model and sedimentation rates

Sediment accumulation rates are 36 m/My for Santonian Zones CC17 and CC16 and 19 m/My for Zone CC15 (Figure **F4**). The interval from the uppermost Coniacian to middle Turonian, encompassing Zones CC14 and CC13, has an average sediment accumulation rate of 63 m/My. Sediment accumulation rates accelerate markedly in the lower to middle Turonian Zone CC12 to a rate of 272 m/My. This estimate does not correct for the hole deviation from vertical (see **Petrophysics** and **Operations**).

Site U1513

Background and objectives

The objectives for coring Site U1513 on the western margin of the MB were to (1) obtain a continuous Late Cretaceous sediment record to better document the rise and fall of the Cretaceous hot greenhouse climate at southern high latitudes (~60°S paleolatitude), (2) characterize how oceanographic conditions changed during the Cenozoic opening of the Tasman Passage and the restriction of the Indonesian Gateway, and (3) obtain basalt from the base of the sedimentary sequence to provide stratigraphic control on the age and nature of the pre-Gondwana breakup succession. A particularly important goal was to obtain a complete OAE 2 sequence across the C/T boundary in order to characterize associated biotic, oceanographic, and climatic changes. The Site U1513 sequence will be compared with coeval Expedition 369 sections cored elsewhere on the MB and other ocean drilling (e.g., Site 258) and industry data from the western Australia margin and in the GAB to identify any regional differences in the geochemical biological responses to the OAEs and Cretaceous and Neogene ocean circulation history.

Lithostratigraphy

The Site U1513 cored section is divided into six lithostratigraphic units, five sedimentary and one igneous, based on a combination of data from Holes U1513A, U1513B, U1513D, and U1513E. Lithostratigraphic units and boundaries are defined by changes in lithology as identified by macroscopic core description, microscopic examination of smear slides and thin sections, and X-ray diffraction (XRD) and X-ray fluorescence (XRF) analyses. Lithostratigraphic Unit I is a 64.93 m thick sequence of light gray to pale yellow calcareous ooze and nannofossil ooze with sponge spicules that is Pleistocene–late Miocene in age. Unit II is a 182.93 m thick sequence of Campanian–Cenomanian white to greenish gray calcareous and nannofossil ooze/chalk and clayey nannofossil chalk with intervals of silicified limestone. Unit III is a 21.87 m thick sequence of alternating greenish gray, light gray, and black nannofossil-rich claystone that is Cenomanian in age. Unit IV is a 187.12 m thick sequence of black claystone and nannofossil-rich claystone that is Cenomanian–Albian in age. Unit V, described only in Hole U1513D, is a 234.25 m thick sequence of sandstone with siltstone and silty claystone that are Aptian to Valanginian in age. Unit VI is an 82.2 m thick alternation of extrusive basalt flows and breccia intruded by a diabase dike. A sharp boundary is present between Units V and VI. The top of Unit VI is defined by a flow-top breccia with an altered matrix that grades downsection into a massive plagioclase-phyric basalt flow. The unit is composed of five extrusive sequences intercalated with four volcaniclastic breccia beds that show graded structures and are defined as lithologic Units 1–7. Each extrusive sequence is generally bounded by chilled margins but also by faults or textural and color changes. Most discrete flows appear to be massive, thin sheets of olivine ± pyroxene- or plagioclase-phyric (some megacrystic) basalt. The least-altered portions of the lowermost sequence (Unit 7) show a higher degree of vesicularity and highly angular vesicles that may indicate subaerial to very shallow eruption depths. A xenolith-bearing diabase dike intrudes the flow sequences. The contact between the xenolith-bearing diabase dike and the extrusives are defined by either faulted or chilled margins with alteration halos. These flows show a lesser degree of alteration in Hole U1513E than in Hole U1513D, and preliminary megascopic and thin section analyses reveal the original porphyritic, microcrystalline, or vesicular textures, with some of the bottom flows showing interesting crosscutting lineation features and absence of minor intrusion intervals.

Biostratigraphy and micropaleontology

Samples from all core catchers from Holes U1513A and U1513D and selected samples from Hole U1513B were analyzed for calcareous nannofossils, planktonic foraminifers, and benthic foraminifers. In addition, samples from split core sections were also evaluated for calcareous nannofossils and/or planktonic foraminiferal assemblages as necessary. Observations of other distinctive and potentially age or environmentally diagnostic microfossil groups, such as organic-walled dinoflagellate cysts (dinocysts), radiolarians, ostracods, fish debris, bryozoans, small corals, and inoceramid prisms were also made in all core catcher samples. Calcareous nannofossil and planktonic foraminiferal datums form the chronologic framework for Site U1513 shallower than 450 m CSF-A.

Calcareous nannofossils

Core 369-U1513A-1H is in calcareous nannofossil Zone CN15 (upper Pleistocene/Holocene), whereas planktonic foraminifers indicate lower Pleistocene Subzone Pt1a. Samples 2H-CC and 3H-CC are assigned to middle Pleistocene Subzone CN14a, whereas Sample 4H-CC is assigned to upper Pliocene Subzone CN12a. Cores 5H through 6H contain mixed assemblages of Neogene and Paleogene species, but the main component of the nannoflora indicates lower Pliocene Zone CN10. The base of Core 7H also contains a mixed assemblage but is dominated by species that indicate a late Miocene age. Sample 8H-CC is calcareous ooze mixed with fragmented Mn oxide nodules and phosphatized limestone that contains a mixed assemblage with species derived from the Upper Cretaceous, Paleogene, and Neogene; thus, it cannot be assigned confidently to a calcareous nannofossil zone. Cores 9H through 15F are assigned to the lowermost Campanian Zone CC17. Upper Santonian Subzone CC16b is found in Core 16X and lower Santonian Subzone CC16a is found in Core 17X. The interval between Cores 18X and 23X is assigned to upper Coniacian Zone CC15. Cores 24X through 28X are assigned to middle to lower Coniacian Zone CC14. The Turonian to

lower Albian succession is described exclusively from Hole U1513D. Sample 369-U1513D-10R-CC is assigned to upper Turonian Zone CC13. The middle to upper Turonian Zone CC12 ranges from Core 11R to Core 14R, whereas Sample 15R-CC is assigned to lower Turonian Zone CC11. Cores 16R through 20R contain a succession that spans the C/T boundary. Cores 20R through 21R are correlated with Subzones CC9c through CC10a of middle to late Cenomanian age. The lower Cenomanian Subzone CC9c is placed between Cores 23R and 27R. Sample 28R-CC indicates upper Albian Subzones CC9a through CC9b. The Core 29R through 31R interval is placed in Subzone CC8d of late Albian age. The middle Albian, comprising combined Subzones CC8b and CC8c, is found in Cores 32R through 36R. Cores 37R through 39R are assigned to Subzone CC8a of early Albian age. Sediments sampled deeper than Core 39R (~440 m CSF-A) were barren of calcareous nannofossils.

Planktonic foraminifers

Planktonic foraminiferal communities span the Pleistocene through late Miocene and unconformably overlay a lower Campanian through Albian sequence. Pliocene planktonic foraminiferal Zones PL5 to PL2 were identified based on the presence of indicative taxa between Samples 369-U1513A-3H-CC and 6H-CC. The interval between Samples 6H-5, 146–150 cm, and 8F-CC, immediately above the unconformity, is assigned to Miocene Zones M14–M11. Beneath the hardground is a lowermost Campanian through Albian sequence. Samples 9H-CC to 10H-CC are unzoned, whereas Samples 11F-CC to 18X-CC; Samples 369-U1513B-13F-2, 89–91 cm, to 14F-CC; and Samples 369-U1513D-5R-CC to 7R-CC (79.8–144.97 m CSF-A) are assigned the Santonian *Planoheterohelix papula* Zone. Samples 369-U1513A-19X-CC to 27X-CC and Samples 369-U1513D-8R-2, 73–75 cm, to 11R-CC are of Coniacian age and represent the interval between the base of the *P. papula* Zone and the top of the *Falsotruncana maslakovae* Zone. The *F. maslakovae* Zone spans Samples 369-U1513A-28X-CC through 32X-CC and 369-U1513D-12R through 15R-CC. Samples between Sample 369-U1513A-33X-CC and 46X-CC and between Samples 369-U1513D-16R-CC and 25R-CC are frequently barren of planktonic foraminifers or have rare, poorly preserved individuals. A middle Cenomanian to late Albian age is inferred from Sample 369-U1513A-46X-CC to the bottom of the hole (284.69 m CSF-A). Hole U1513D extends beyond the base of Hole U1513A and can be divided into the upper Albian *Thalmanninella appenninica, Pseudothalmanninella ticinensis,* and *Biticinella breggiensis* Zones. Deeper than Sample 369-U1513D-33R-CC, samples are predominantly barren of planktonic foraminifers.

Benthic foraminifers

The Cenozoic benthic foraminiferal assemblages recorded in Cores 369-U1513A-1H through 8F are characterized by abundant calcareous-walled taxa. The species present indicate a bathyal water depth. Two distinctively different benthic foraminiferal assemblages were recorded from the Cretaceous strata. In Cores 9H through 36X, a bathyal benthic assemblage dominated by calcareous-walled forms was recorded. The percentage of planktonic foraminifers relative to benthic forms in this interval fluctuates between 80% and 99%. In the Turonian strata, there is a decrease in the number of planktonic individuals, and the percentage of planktonic foraminifers drops to 40% (Cores 28X through 42X). Agglutinated foraminifers dominate from Samples 34X-CC through 50X-1, 126–127 cm, and 369-U1513D-22R-CC through 40R-CC. *Glomospira* spp. is the most common taxon within this interval, suggesting a bathyal water depth.

Paleomagnetism

The NRM of all archive-half core sections and 98 discrete samples collected from the working halves of Holes U1513A, U1513B, U1513D, and U1513E was measured. The archive halves were stepwise treated with up to 20 or 30 mT AF demagnetization and measured with the pass-through SRM at 5 cm intervals. Discrete samples were progressively demagnetized up to 60 or 80 mT and measured with the spinner magnetometer or the SRM. The NRM intensity of the recovered cores is in the order of 10^{-5} to 1 A/m and broadly covaries with lithology. The calcareous ooze/chalk in the upper part and the basalt in the basal part of Hole U1513D display the weakest and the strongest NRM intensity, respectively. Despite the weak NRM of the calcareous ooze/chalk, the demagnetization results after 20 mT showed inclination zones of dominant positive and negative values, defining a magnetic polarity sequence from Chrons C1n to C2An.3n for the uppermost ~65 m. The inclinations of the ~65 to 455 m CSF-A interval are mostly scattered, and dominant negative values from 200 to 450 m CSF-A indicate a normal polarity, which is assigned to Chron C34n based on shipboard biostratigraphy. The inclinations deeper than 455 m CSF-A exhibit a distinct pattern of zones of either positive or negative values, establishing a well-defined magnetic polarity sequence. The polarity sequence between 455 and ~690 m CSF-A is tentatively correlated with Chrons M0r–M10n, indicating the absence of most of the Aptian strata and increasing sedimentation rates between ~530 and ~690 m CSF-A. The well-defined reversed and normal polarities deeper than ~690 m CSF-A occur in the basalt unit and cannot be correlated with the geomagnetic polarity timescale (GPTS) without constraints of ages from the basalt.

Petrophysics

Physical property data were obtained with the WRMSL, NGRL, PWC, SHMSL, and discrete samples. The uppermost 35 m preserves cyclicity in NGR (~15 counts/s amplitude; ~5 m thickness) and was deconvolved into U, Th, and K concentrations. The C/T boundary interval shows a distinct plateau of ~40 counts/s in NGR values at ~240–245 m CSF-A. Additionally, NGR values preserve a broad trend to higher counts through a mudstone interval spanning from 230 to 455 m CSF-A with a trough near 320 m CSF-A (Figure **F5**). Below a contact with underlying volcaniclastic sandstones at 455 m CSF-A, NGR values decrease by nearly an order of magnitude from 75 to 10 counts/s and magnetic susceptibility values increased by two orders of magnitude from ~10 to ~1000 counts/s. Similarly, both grain and bulk density step to higher values across this transition. NGR values, more specifically U content, spike across an interval near 675 m CSF-A, possibly signifying abundant terrestrial organic matter. The indurated breccia and crystalline rocks of lithostratigraphic Unit VI show spikes in magnetic susceptibility and density, along with nearly undetectable counts of NGR. In the overlying sedimentary sequence (Units I–V), trends in porosity and PWC measurements demonstrate a gradual but occasionally punctuated change to lower and higher values, respectively.

Downhole logging was conducted in Holes U1513A, U1513D, and U1513E using several downhole tool configurations, including the modified triple combo tool string, which measures NGR, density, sonic velocity, and resistivity; the traditional triple combo; the Formation MicroScanner (FMS) with the porosity tool; and the Versatile Seismic Imager for some intervals in Hole U1513E. NGR, density, and resistivity measurements from each hole yielded similar results for the overlapping depth intervals across Holes U1513A, U1513D, and U1513E. The most continuous downhole logging run using the triple combo occurred in Hole U1513E and spanned from

a bridge at ~615 m WMSF to the bottom of the drill pipe at ~119 m WMSF. The wireline logging data provided continuous coverage and filled several coring gaps. The most striking features include a strong positive response in resistivity, density, and sonic velocity values through intervals of silicified limestone (96–123 and 152–180 m WMSF; lithostratigraphic Unit II) and a shift from low to high NGR across the C/T boundary interval (~240–245 m WMSF). NGR increases downhole from this horizon through the Cenomanian–Albian claystones, displaying similar trends to the core-based NGR. In situ temperature measurements were attempted in Hole U1513B, but this experiment returned only one reliable measurement of 4.55°C from Core 369-U1513B-5H.

Geochemistry

The Site U1513 geochemistry program was designed to characterize interstitial water and bulk sediment composition and to assess the potential presence of volatile hydrocarbons for routine safety monitoring. Samples were taken from Holes U1513A and U1513D. All 90 headspace gas samples showed only low concentrations of methane (≤60 ppmv) and trace levels of ethane and propane.

For interstitial water analyses, 60 samples were recovered from squeezing 10 cm whole rounds, covering 0–366.4 and 471.8–687.3 m CSF-A. Sample salinity was generally constant, with the exception of distinctly fresher interstitial water between 281.8 and 303.0 m CSF-A; this exception is also seen in the Br^- and Cl^- profiles and may reflect a low-salinity water source in this interval. The dissolved Mg, K, and Na concentration profiles reflect alteration of volcanic material found in lithostratigraphic Units IV and V. No evidence for significant sulfate reduction was detected; sulfate is present throughout, and Ba concentrations are correspondingly low. The dissolved Ca (Figure **F5**) and Sr concentration profiles primarily reflect the release of these elements during the alteration reactions of volcanic material. Li appears to have been released in Unit IV and then is incorporated into alteration products in Unit V. Dissolved Si reflects the presence of biogenic opal-A in Units I and II; lower concentrations in Units III and V may reflect the opal-A/CT and CT to quartz transition, respectively. Elevated Mn concentrations demonstrate the reducing character of the sedimentary sequence below Unit I.

In addition, 129 bulk sediment samples were collected downhole to ~690 m CSF-A (Core 369-U1513D-65R), the contact with igneous material. Additional samples were measured at a higher resolution through the putative OAE 2 and 1d intervals. $CaCO_3$ content varies from 0 to 93 wt%, reflecting variations in lithology. TOC was broadly <1 wt% except in the OAE 2 interval, where TOC reaches 10.5 wt%. TN is generally below the detection limit. A total of 57 samples with TOC ≥ 0.8 wt% from the OAE 2 and 1d intervals were analyzed with the source rock analyzer. Samples with higher concentrations of TOC (>3 wt%) were found to be predominantly marine in source, whereas the lower TOC samples were generally inconclusive.

Stratigraphic correlation

Four holes were cored at Site U1513. Recovery in any one hole ranged from poor to excellent, but when combined, overall recovery was excellent for most of the interval that penetrated and spanned the Valanginian through the present day. Splices were constructed for the 0–95 m core composite depth below seafloor (CCSF) intervals (Holes U1513A and U1513B) and from 220 to 295 m CCSF (Holes U1513A and U1513D) (Figure **F5**). These splices cover the late Miocene through recent and the middle Cenomanian through the middle Turonian, respectively, as estimated from bio- and magnetostratigraphy. Portions of both splices were formed by appending subsequent cores from the same hole because of aligned core breaks or poor recovery in the other hole (i.e., there was no bridge across core breaks in these intervals). However, correlation to downhole logging data minimized the uncertainty introduced by this approach. The 95–220 m CSF-A interval was recovered in Holes U1513A and U1513D. Despite this, no splice was attempted because recovery was too low to meaningfully correlate at the meter scale in this interval, but pooled data suggest recovery should be sufficient to generate good records with 1 My resolution. The interval from 295 to 757.4 m CSF-A was only cored in Hole U1513D, but recovery was generally very good to excellent, averaging 82% across ~70 m of basalt and basaltic breccia (lithostratigraphic Unit VI) and 75% over the 395 m of overlying sandstones and claystones (Unit V) between the basalt and the lower splice. The oldest biostratigraphic date for these overlying sediments is middle Albian, although magnetostratigraphy suggests portions could be older.

Age-depth model and sedimentation rates

Sediment accumulation rates are presented in Figure **F5** for the Albian through Campanian portion of Site U1513. Sediment accumulation rates averaged ~12 m/My from the Albian through Coniacian but dropped appreciably during the Santonian and lower Campanian to only 8 m/My, with an apparent rate of only 3 m/My in the Santonian. Alternatively, part of the Santonian may be missing due to a hiatus in sediment accumulation. Sediment accumulation rates deeper than 450 m CSF-A are based on the paleomagnetic record. Sediment accumulation rates for the Barremian to upper Hauterivian (M0 to base Mr8) averaged approximately 10 m/My, whereas estimated rates for the lower Hauterivian and Valanginian (M9 to M10) were ~132 m/My.

Site U1514

Background and objectives

Site U1514 is the northernmost and deepest site targeted during Expedition 369. The greater paleodepth of the site relative to other sites cored in the MB provides the opportunity to characterize the evolution of deep-water masses and deep ocean circulation during the final phase of breakup among the Gondwana continents. Because Site U1514 was located at a high paleolatitude (~60°S), the sediments preserve a paleoclimate record that serves as a highly sensitive monitor of global climatic changes. The site was expected to sample a series of Cenozoic and possibly Late Cretaceous sedimentary drifts and erosional features that would enable greater insight into the early and later phases of the opening of the Tasman Gateway and restriction of the Indonesian oceanic gateway. The current seabed is composed of Paleogene/Neogene/Quaternary oozes that sit unconformably on the Cretaceous (Maloney et al., 2011).

The primary objectives for coring Site U1514 were to (1) obtain a continuous Cenozoic sediment record in the MB to characterize how oceanographic conditions changed during the Cenozoic opening of the Tasman Passage and the restriction of the Indonesian Gateway; (2) reconstruct middle through Late Cretaceous paleotemperature changes to document initiation of the Cretaceous hot greenhouse climate, the duration of extreme warmth, and when a switch to a cooler climate occurred; and (3) obtain a complete and well-preserved sediment record across mid-Cretaceous OAEs to better understand their cause and accompanying changes in the climate-ocean system and the marine biota.

Lithostratigraphy

The Site U1514 cored section is divided into three main lithostratigraphic units based on data from Holes U1514A and U1514C, with Units I and III further divided into two subunits (Figure **F6**). Lithostratigraphic units and boundaries are defined by changes in lithology as identified by macroscopic core description, microscopic examination of smear slides, and XRD and XRF analyses. Lithostratigraphic Unit I is a 81.20 m thick sequence of very pale brown to pale yellow nannofossil ooze, foraminiferal ooze, and sponge spicule–rich nannofossil ooze that is Pleistocene–Eocene in age. The unit is divided into Subunits Ia and Ib at 30.38 m CSF-A in Hole U1514A. Subunit Ib spans the Miocene–Eocene and differs from Subunit Ia in that it is characterized by an increased abundance of sponge spicules. Further, the color of Subunit Ib changes to yellow-brown, which is distinctively darker than Subunit Ia. Unit II is a 308.01 m thick sequence of Eocene–Paleocene light greenish gray clayey nannofossil ooze, sponge spicule–rich clay, and nannofossil-rich clay that gradationally transitions into clayey nannofossil chalk and nannofossil-rich claystone. Unit III is a 126.43 m thick sequence of greenish gray, brown, and black claystone that is Paleocene–Albian in age. Unit III is divided into Subunits IIIa and IIIb at 454.33 m CSF-A in Hole U1514C. Subunit IIIb was deposited during the Cenomanian/Albian to Albian and is distinguished from overlying Subunit IIIa (Paleocene to Cenomanian/Albian) in that it is characterized by darker greenish gray/black claystone. Soft-sediment deformation, possibly slumping, includes convoluted and overturned bedding and is also present in Subunit IIIa (Cores 369-U1514C-25R through 29R; 411.2–455.31 m CSF-A).

Biostratigraphy and micropaleontology

Samples from core catchers in Holes U1514A and U1514C were analyzed for calcareous nannofossils, planktonic foraminifers, and benthic foraminifers. As necessary, additional samples from split-core sections were evaluated for calcareous nannofossils and/or planktonic foraminiferal assemblages. Observations of other distinctive and potentially age or environmentally diagnostic microfossil groups including calcispheres, diatoms, radiolarians, fish debris, sponge spicules, and inoceramid prisms were also recorded.

The Hole U1514A nannofossil biostratigraphy spans from Pliocene Subzone CN12a to lower Eocene Subzone CC9b, whereas Hole U1514C spans middle Eocene Subzone CP13b to Subzones CC8b–CC8c of the early Albian. Planktonic foraminiferal assemblages recovered at Site U1514 are generally rare with poor to moderate preservation, although discrete samples in the Pleistocene, Paleocene, Turonian, and Albian contain seemingly unrecrystallized specimens. Planktonic foraminiferal communities in Hole U1514A span Pleistocene Subzone Pt1a through lower Eocene Zone E4. Hole U1514C ranges from middle Eocene Zones E8–E9 to the *T. appenninica/P. ticinensis* Zones of the upper Albian. An apparently complete (at least to biozone level) though bioturbated Cretaceous/Paleogene (K/Pg) boundary section was recovered in Core 369-U1514C-23R. Benthic foraminiferal assemblages are dominated by epifaunal, calcareous-walled taxa, indicating bathyal to abyssal paleowater depths throughout the recovered interval.

Paleomagnetism

The NRM of all archive-half core sections and 82 discrete samples collected from the working halves in Holes U1514A and U1514C was determined as part of the paleomagnetism measurement program (Figure **F6**). The archive halves were stepwise treated with up to 20 or 30 mT AF demagnetization and measured with the pass-through SRM at 5 cm intervals. Discrete samples were progressively demagnetized up to 60 mT and measured with the SRM. The NRM intensity of the recovered cores is in the order of 10^{-6} to 1 A/m and broadly covaries with lithology. Inclinations after the 20 mT demagnetization step exhibit intervals dominated by positive and negative inclination values, defining an almost complete magnetic polarity sequence from Chron C1n (Brunhes) to Chron C34n, the long Cretaceous Normal Superchron, with 74 identified and dated reversals. The magnetic data are of excellent quality in the advanced piston corer (APC) section (0–95 m CSF-A) and exhibit larger scatter caused by drilling disturbance in the extended core barrel (XCB) and RCB cores. The sequence is interrupted by four hiatuses at 11, 18, 30, and 41 m CSF-A identified by sharp lithologic boundaries in conjunction with biostratigraphic constraints.

Petrophysics

Magnetic susceptibility, GRA density, NGR, thermal conductivity, *P*-wave velocity, color reflectance spectroscopy and colorimetry (RSC), and MAD were measured on whole-round sections, split-core sections, and discrete samples from Site U1514. Several unique features were identifiable using the physical property data, including distinct signals in the NGR (Figure **F6**), magnetic susceptibility, and GRA density near the C19r event (~152 m CSF-A), the Paleocene–Eocene interval (~275–280 m CSF-A), the Cretaceous/Paleogene boundary (382–415 m CSF-A), and the Cenomanian–Turonian interval (415–445 m CSF-A). However, the latter is within a zone of soft-sediment deformation possibly associated with slumping.

Magnetic susceptibility values vary between 1.76 and 50.48 IU and consist of sections of high- and low-frequency variations downhole. Bulk density estimated from GRA ranges from 1.6 to 1.9 g/cm^3. NGR ranges from 0 to 105 counts/s with high-amplitude cyclic fluctuations downhole, which is coincident with changes in sediment RSC. The bulk density, grain density, and porosity of cored material were measured on discrete samples (MAD). These data show several deviations from the expected trend. In several sections, porosity increases with depth. This increase may reflect lithologic changes and/or is associated with soft-sediment deformation that may have led to several packages of material being more over- or undercompacted than the surrounding beds. *P*-wave velocities range from ~1500 m/s near the seafloor to ~2100 m/s at ~290 m CSF-A. Velocity tends to decrease below this depth to 1800–1900 m/s at the bottom of the hole (515.7 m CSF-A), except for the 390–470 m CSF-A interval, where velocities are scattered between 1800 and 2300 m/s, which brackets the zone with soft-sediment deformation.

Downhole logging was conducted in Hole U1514C using the modified triple combo tool string. The measurements yielded similar results for the overlapping depth intervals when core recovery was good. The downhole tools provided continuous coverage of the borehole and filled several coring gaps. The most striking features include several peaks in NGR at ~395, ~425, and ~445 m WMSF and between 455 and 480 m WMSF. Interestingly, the two peaks in the NGR log at ~395 and ~425 m WMSF correspond to a decrease in bulk density, sonic velocity, and resistivity, as well as more clay rich lithofacies. There are also notable slower sonic velocities between 420 and 440 m WMSF, which could (at least partially) reflect a thick zone of soft-sediment deformation associated with possible slumping. Magnetic susceptibility data were collected in Hole U1514C, but the signal quality was poor. In addition, in situ temperature measurements were obtained in Hole U1514A and were

combined with the thermal conductivity data to determine heat flow (45–49 mW/m^2).

Geochemistry

The Site U1514 geochemistry program was designed to characterize the composition of interstitial water and bulk sediments and to assess the potential presence of volatile hydrocarbons for routine safety monitoring. Samples were taken from Holes U1514A and U1514C. A total of 56 headspace gas samples were taken, with only low concentrations of methane (≤90 ppmv) and trace levels of ethane detected.

For interstitial water analyses, 54 samples were recovered from whole-round squeezing of sediment intervals from Holes U1514A (0–247.7 m CSF-A) and U1514C (255.0–515.7 m CSF-A). Sample salinity is generally constant, with the exception of distinctly fresher interstitial water in lithostratigraphic Subunit IIIa (Figure **F6**). This low-salinity interval reflects decreased concentrations of many elemental profiles, particularly Br^- and Cl^-, and an input of fresher water. The dissolved Mg, K, Ca, Li, Sr, and Na concentration profiles reflect alteration of volcanic material from depths below the cored interval for Site U1514. Moderate sulfate reduction was detected because sulfate is present but decreases with depth, and Ba concentrations are correspondingly low. Dissolved Si reflects the presence of biogenic opal-A in lithostratigraphic Units I and II and the top part of Subunit IIIa; lower concentrations at the bottom of Subunit IIIa and in Subunit IIIb may reflect the opal-A/CT transition. Periodic elevated Mn and Fe concentrations demonstrate the reducing character of the sedimentary sequence at certain intervals at this site.

A total of 64 bulk sediment samples were collected downhole to ~513 m CSF-A (Core 369-U1514C-35R). Additional samples were measured from the putative OAE 2 and 1d intervals. $CaCO_3$ content varies from 0 to 90 wt%, reflecting variations in lithology (Figure **F6**). TOC is generally less than 0.3 wt%, except in the OAE 1d interval where TOC reached 1.2 wt%. TN is generally below the detection limit. A total of 8 working-half samples from the potential OAE 2 and 1d intervals were analyzed on the source rock analyzer. Although the lower TOC content samples were generally inconclusive, kerogen in samples with higher concentrations of TOC (>1 wt%) were found to be predominantly terrestrial in source.

Stratigraphic correlation

Three holes were cored at Site U1514. Recovery in Hole U1514A was excellent (near 100%), and the total recovery of Holes U1514A and U1514C was 65%. Target depths were recommended before and during the coring of Hole U1514C, which aided the bridging of coring gaps in Hole U1514A. A splice was created for the overlapping portion of the lower Eocene, spanning 195.6 to 266.1 m CCSF in Holes U1514A and U1514C. This splice was established by identifying similar trends in NGR and subsequent comparison of high-resolution physical property data. Recognition of sharp peaks in NGR enabled correlation of core data to wireline logging results and confirmed the accuracy of the splice.

Together, Holes U1514A and U1514C span the end-Albian to the present, with good coverage over much of the Paleogene and Upper Cretaceous, including a seemingly complete record over the K/Pg boundary in Core 369-U1514C-23R. Downcore, a multicolored interval of deformed sediments spanning Cores 25R through 29R is consistent with the downslope motion of the upper portion of the sequence at this site.

Age-depth model and sedimentation rates

Sediment accumulation rates vary throughout the section, with the lowest values recorded in the Neogene and Cretaceous (3–9 m/My) and the highest values (13-15 m/My) recorded in the Eocene and Paleocene (Figure **F6**). Major unconformities are present in the lower Pleistocene, Pliocene, Miocene, and Oligocene. The sediment accumulation rate is quite low for the Oligocene and Miocene interval (~0.13 cm/ky), moderate for the Eocene and Paleocene interval (~1.0 cm/ky), and modest for most of the Cretaceous interval (~0.29 cm/ky).

Site U1515

Background and objectives

Site U1515 is the westernmost and shallowest site targeted during Expedition 369 with the primary objective to provide evidence of the prebreakup rifting history in the region prior to the final separation of Greater India and Antarctica. The site location was chosen based on seismic evidence of dipping strata below what is interpreted to be the eastward extension of the Valanginian unconformity cored at Site U1513 in the western MB. The extrusive basalts that cover this unconformity in the western MB are not present at Site U1515.

Structural interpretations suggest that depocenters in the eastern MB are older (Permian? to Jurassic) than those in the western MB (Jurassic?) (Borissova et al., 2002). Site U1515 is the first sampling of this eastern depocenter and will test the hypothesis of early Mesozoic rifting. Cores recovered from this site will enable the investigation of the tectonic and structural relationships with similarly aged rifts along the western margin of Australia, in particular the adjacent Perth Basin (Bradshaw et al., 2003), and rift structures in Antarctica (Maritati et al., 2016). Finally, the cored record will ascertain the provenance of these earlier (Jurassic?) sediments as possibly sourced from the Pinjarra orogen or Albany-Frazer province.

Lithostratigraphy

The cored section of Hole U1515A, the only hole at Site U1515, is divided into two main lithostratigraphic units (I and II; Figure **F7**), which are further divided into five subunits (Ia, Ib, IIa, IIb, and IIc). Lithostratigraphic units and boundaries are defined by changes in lithology as identified by macroscopic core description, microscopic examination of smear slides and thin sections, and XRD and XRF analyses. Unit thicknesses are not given because of the overall low core recovery. Lithostratigraphic Unit I (Cores 1R through 15R) is a sequence of calcareous ooze/chalk with sponge spicules, silicified limestone, bioclastic limestone, chert, sandy limestone, and sandstone (arkose). Subunit Ia (Cores 1R through 8R) consists of light greenish gray calcareous ooze with sponge spicules, whereas Subunit Ib (Cores 9R through 15R) is generally more lithified and consists largely of calcareous chalk and 10–40 cm thick silicified limestone with frequent chert beds. Because of poor recovery in this interval, the contact between Units I and II was not recovered. Unit II (Cores 24R through 55R) largely consists of gray to black silty sand and glauconitic sandstones/silty sandstones. Subunit IIa (Cores 24R through 36R) is characterized by abundant glauconite and consists of black to greenish gray silty sand and sandstone. Subunit IIb (Cores 37R through 41R) consists largely of fine- to coarse-grained sandstones with interbedded siltstone and claystone. This subunit differs from Subunit IIa in that it contains less glauconite and more abundant pyrite nodules. Subunit IIb gradually transitions to organic-rich silty sandstone and claystone with coal and

plant debris, which are characteristic components of Subunit IIc (Cores 44R through 55R). The sediments recovered in Unit II are possibly terrestrial in origin.

Biostratigraphy and micropaleontology

Hole U1515A core catcher samples were analyzed for calcareous nannofossils, planktonic foraminifers, and benthic foraminifers. Observations were recorded for other distinctive and potentially age or environmentally diagnostic microfossil groups, including calcispheres, radiolarians, pollen grains and spores, fish debris, sponge spicules, and inoceramid prisms.

Microfossils occur in the upper part of the hole (Cores 1R through 15R), whereas the lower part (Cores 16R through 49R; no samples were taken deeper than Core 49R) is barren of all calcareous and siliceous microfossil groups. However, a spore found in a smear slide of Sample 39R-1, 97 cm, was identified as *Contignisporites* sp. (likely *Contignisporites glebulentus*), which could indicate an age of Pliensbachian or younger. Most of the Neogene and Paleogene samples (Cores 1R through 14R) indicate reworking of Pliocene, Miocene, Oligocene, and Eocene species. The nannofossil biostratigraphy of Hole U1515A spans from upper Pleistocene Subzone CN14b to upper Campanian Zone CC22. Planktonic foraminiferal assemblages are in good agreement with this stratigraphic determination, spanning from the upper Pleistocene Subzone Ptlb through the late Campanian/late Santonian *Globigerinelloides impensus* Zone. Benthic foraminiferal assemblages indicate an outer neritic to upper bathyal paleodepth throughout the analyzed interval (Figure **F7**).

Paleomagnetism

The NRM of most of the archive-half core sections and 19 discrete samples collected from the working halves of Hole U1515A was determined (Figure **F7**). The archive halves were stepwise treated with up to 20 mT AF demagnetization and measured with the pass-through SRM at 5 cm intervals. Discrete samples were progressively demagnetized up to 60 mT and measured with the SRM. The NRM intensity of the recovered cores is in the order of 10^{-5} to 1 A/m and broadly covaries with lithology. Inclinations after the 20 mT demagnetization step exhibit intervals dominated by positive and negative inclination values, defining a brief magnetic polarity sequence from Chron C1n (Brunhes) to Subchron C1r.2r. Although the magnetic record is noisy and the core recovery is poor, intervals of predominantly normal and reversed polarity can be discerned in the remainder of the sections deeper than 20 m CSF-A. However, a correlation to the GPTS is not possible mainly because of the poor core recovery and the lack of biostratigraphic control.

Petrophysics

Site U1515 had overall low core recovery (18%), so physical property data is sparse and discontinuous, particularly between ~130 and ~270 m CSF-A. Despite the quality of the record, the data show very broad trends from the top to the bottom of the hole, and some comparisons can be made between physical property data and lithology, including a general increase in *P*-wave velocity and thermal conductivity, which corresponds to a change from unlithified to weakly lithified glauconitic sand, sandstone and interbedded siltstone, and claystone (lithostratigraphic Subunits IIa and IIb) to silty sandstone and claystone with coal and plant debris (Subunit IIc). This change in velocity also corresponds to a 364–373 m CSF-A unconformity identified in seismic images. Other broad trends include an overall increase in thermal conductivity, an increase in bulk and grain densities, and an overall decrease in porosity. The color reflection and bulk density data are noisy, but they show some trends that can be correlated with lithostratigraphic units. Similarly, the NGR (Figure **F7**) and magnetic susceptibility data also show broad trends and potentially highlight zones where changes in lithology occur (e.g., the highest magnetic susceptibility values, high bulk density, and low NGR values at ~270 m CSF-A correspond to glauconitic sandstone).

Geochemistry

The Site U1515 geochemistry program was designed to characterize the composition of interstitial water and bulk sediments and to assess the potential presence of volatile hydrocarbons for routine safety monitoring. No gas was detected in the 38 headspace gas samples that were taken.

For interstitial water analyses, 17 samples were recovered from whole-round squeezing of sediment intervals at 2.9–77.1 and 287.8–441.60 m CSF-A. Sampling was restricted due to low core recovery at Site U1515, which limits interstitial water interpretation. Sample salinity is generally constant, and alkalinity generally decreases downhole. The dissolved Mg, K, and Ca concentration profiles possibly reflect alteration of volcanic material from depths below the cored interval for this site. Increasing Sr concentrations with depth in lithostratigraphic Unit I may indicate carbonate recrystallization. Low levels of sulfate reduction were detected; sulfate is present but decreases with depth. Dissolved Si reflects the presence of biogenic opal-A in Unit I; lower concentrations in Unit II indicate the interval falls below the opal-A/CT transition (Figure **F7**). Elevated Mn and Fe concentrations in Unit II demonstrate the reducing character of the sedimentary sequence in that interval.

A total of 33 bulk sediment samples were collected downhole to ~511 m CSF-A (Core 369-U1515A-55R). Within the intervals with carbon-rich layers, small chips were taken from the carbon-rich parts for analysis. Carbonate content is very high (~80–90 wt%) in the upper part but drops to nearly 0 wt% deeper than 160 m CSF-A (Figure **F7**). Lithostratigraphic Subunit IIa and shallower contains 0–2.4 wt% TOC, whereas Subunits IIb and IIc contain as much as 46.2 wt% TOC (likely coal fragments). TN is <0.05 wt% in Subunits Ia, Ib, and IIa but exceeds 0.3 wt% at four horizons in Subunits IIb and IIc, showing a pattern similar to that of TOC. In most samples with higher TOC (>1 wt%), the kerogen was found to be predominantly terrestrial in origin, except for the ~430–460 m CSF-A interval, where a more significant algal contribution is suggested.

Site U1516

Background and objectives

Site U1516 is located in the south-central MB. Objectives for drilling at Site U1516 were to (1) obtain a continuous and expanded Cenozoic and Upper Cretaceous pelagic carbonate sediment record in the MB to reconstruct climatic shifts across the rise and fall of the Turonian and early Eocene hot greenhouse climates, (2) determine the relative roles of productivity, ocean temperature, and ocean circulation at high southern latitudes during Cretaceous anoxic events and across the PETM, and (3) characterize how oceanographic conditions changed during the Cenozoic opening of the Tasman Passage and the restriction of the Indonesian Gateway. The Site U1516 sequence will be compared with coeval Expedition 369 sections cored elsewhere on the MB and with other IODP and industry data from the southern and western Australia margins to correlate recovered lithologies with seismic lines across the MB and to identify regional differences in the geochemical biological responses to the OAEs, Cretaceous, Paleogene, and Neogene ocean circulation history.

Lithostratigraphy

Site U1516 is divided into four main lithostratigraphic units (I, II, III, and IV; Figure F8), with Unit I divided into three subunits (Ia, Ib, and Ic). Lithostratigraphic units and boundaries are defined by changes in lithology as identified by macroscopic core description, microscopic examination of smear slides and thin sections, and XRD and XRF analyses. Lithostratigraphic Unit I is a sequence of calcareous/foraminiferal/nannofossil oozes and chalks with sponge spicules that is Pleistocene to Paleocene in age. Subunit Ia consists of pinkish white, pinkish gray, and very pale orange sponge spicule–rich calcareous oozes that are Pleistocene to Miocene in age. Subunit Ib consists of sponge spicule–rich calcareous chalks and calcareous chalks with sponge spicules that span the Miocene to Eocene. The transition between Subunits Ia and Ib is defined by a shift to higher NGR and bulk density values and a decrease in L* values. Subunit Ic, Paleocene in age and consisting of claystones, is likely to be a condensed interval. An unconformity between the Paleocene and the Turonian marks the boundary between Units I and II. Unit II is calcareous chalk interbedded with chert that gradually transitions into light greenish gray and greenish gray nannofossil chalk with clay that is also interbedded with chert. The boundary between Units II and III is placed at the C/T boundary and is marked by the first occurrence of black laminated claystone at the top of Unit III. Unit III is an alternating sequence of black, greenish gray, and gray claystone (sometimes with abundant nannofossils) and clayey nannofossil chalk with occasional parallel laminations. Unit IV ranges from the Cenomanian to the Albian and is a sequence of black and dark greenish gray nannofossil-rich claystone and claystone with nannofossils with subtle alternations in color throughout.

Biostratigraphy and micropaleontology

Coring at Site U1516 recovered a succession of sediments from the Albian through the Pleistocene. Calcareous nannofossils, planktonic foraminifers, and benthic foraminifers occur throughout this succession, with preservation and abundance sufficient to provide biostratigraphic and paleoecologic information for the entire section. Calcareous nannofossils are abundant to common throughout the section, with barren samples only in the middle Albian and associated with the C/T boundary. Preservation is generally good to moderate, with poor preservation associated only with a condensed Paleocene sequence. Reworking of Paleogene taxa into the Neogene assemblages is common. Preservation of planktonic foraminifers is generally good at Site U1516, with some samples in the upper Albian ranked as excellent. Abundance is more variable; the Neogene, Paleogene, and Turonian generally contain abundant planktonic foraminifers, whereas the Albian contains only rare specimens. Benthic foraminiferal abundance and preservation are also variable. In general, examination of benthic foraminifers indicates a bathyal paleodepth during the Albian through Cenozoic.

Paleomagnetism

We measured the NRM of all archive-half core sections from Holes U1516A, U1516C, and U1516D (Figure F8). The archive halves were stepwise treated with up to 20 mT AF demagnetization and measured with the pass-through SRM at 5 cm intervals. The NRM intensity of the recovered sedimentary cores is in the order of 10^{-6} to 10^{-1} A/m, and lithostratigraphic Unit I, which consists of mainly calcareous oozes and chalk, generally displays weak magnetism. Despite the weak NRM of the calcareous oozes/chalk of Unit I, inclinations after 20 mT demagnetization show zones of dominantly positive and negative values, defining a magnetic polarity sequence from Chrons C1n (Brunhes) through C22r for the upper ~430 m interval, with a total of 84 identified and dated reversals. The magnetic polarity sequence is interrupted by a sedimentary hiatus at ~270 m CSF-A based on biostratigraphic constraints. Below ~430 m CSF-A, inclinations of Units II–IV, which mainly consist of claystones, exhibit predominantly negative values, indicating a normal polarity. The normal polarity zone spans from ~430 to 525 m CSF-A and is assigned to Chron C34n, the long Cretaceous Normal Superchron, based on shipboard biostratigraphic analysis.

Petrophysics

Site U1516 physical property data were collected from Holes U1516A, U1516C, and U1516D. Thermal conductivity shows a minor overall increase downhole, whereas porosity and *P*-wave velocity show a minor overall decrease downhole. In comparison, there is very little variation of bulk and grain density downhole. Exceptions are within the interval between 380 and 460 m CSF-A, which shows a pronounced excursion toward higher values in bulk density, thermal conductivity, and *P*-wave velocity; a minor excursion toward higher values in grain density; and a strong excursion to lower values in porosity. This interval also corresponds to an interval of relatively high magnetic susceptibility and the top of an interval of increasing NGR (Figure F8). Despite the strong correlation between physical properties, this interval does not correlate to lithostratigraphic unit boundaries. NGR and magnetic susceptibility show similar overall trends throughout Site U1516, increasing when the lithology becomes richer in detrital components. At the transition between lithostratigraphic Units II and III (~470 m CSF-A), both NGR and magnetic susceptibility increase when approaching the black shale interval related to OAE 2. Enrichment in U is notable after deconvolution of the NGR. In Unit IV, similar features have been found in the evolution of both proxies with Site U1513, allowing correlations between these two sites.

Geochemistry

The Site U1516 geochemistry program was designed to characterize the composition of interstitial water and bulk sediments and to assess the potential presence of volatile hydrocarbons for routine safety monitoring. No gas was detected in the 57 headspace gas samples that were taken.

For interstitial water analyses, 52 samples were recovered from whole-round squeezing from Holes U1516A (0–223.6 m CSF-A) and U1516C (244.0–541.6 m CSF-A). Sample salinity is generally constant, with the exception of distinctly fresher interstitial water in lithostratigraphic Unit IV (Figure F8). This low-salinity interval reflects decreased concentrations in many elemental profiles, particularly Br^- and Cl^-, and an input of fresher water. The dissolved Mg, K, and Ca concentration profiles possibly reflect alteration of volcanic material from depths below the cored interval for this site. The Sr profile likely reflects carbonate diagenesis. Low levels of sulfate reduction were detected; sulfate is present but decreases with depth. Dissolved Si reflects the presence of biogenic opal-A in lithologic Subunit Ia; decreasing concentrations deeper than Subunit Ib indicate the opal-A/CT transition. Elevated Mn (Figure F8) and Fe concentrations in parts of Subunits Ia and Ib and Units II–IV demonstrate the reducing character of the sedimentary sequence in these intervals.

A total of 43 bulk sediment samples were collected downhole to ~540 m CSF-A. Additional samples were measured from the suggested OAE 2 interval. $CaCO_3$ content varies from 0 to 94 wt%, re-

flecting variations in lithology. TOC is 0–1.2 wt%, except in the OAE 2 interval where TOC reaches 14 wt%. TN is generally below the detection limit.

Eleven samples including one from the putative OAE 2 black shale were also analyzed using the source rock analyzer. The sample from the top of the 8 cm thick black interval indicates Type II kerogen, whereas samples with low (<2 wt%) TOC from the OAE 2 interval and Unit IV are composed primarily of Type IV kerogen. T_{max} values indicate thermal immaturity.

Stratigraphic correlation

Cores from Hole U1516A provide a 225 m thick, continuous record of middle Miocene to recent deposition, and the sequence seems to be biostratigraphically and magnetostratigraphically complete. In Hole U1516C, coring gaps limit knowledge of the lower Miocene, much of the Oligocene, and portions of the Eocene at this site, but both the Oligocene/Miocene boundary interval and a 30 m long interval of the upper Eocene were well recovered. In addition, much of the Upper Cretaceous, all of the Paleocene, and much of the lower and middle Eocene are either missing or represented in a 15 m thick interval of condensed deposition and/or erosion and nondeposition spanning from Section 369-U1516C-26R-4, 106 cm, to the top of Core 25R. In contrast, an excellent record of the upper Albian to the middle Turonian was recovered between Holes U1516C and U1516D, including a seemingly complete splice across the OAE 2 interval.

Age-depth model and sedimentation rates

The Neogene has an average sediment accumulation rate of ~18 m/My from the Pleistocene through the upper Miocene (Figure **F8**). Much of the middle and lower Miocene are missing at a disconformity with an estimated 8 My hiatus. The lowermost Miocene and uppermost Oligocene are present at this site, separated from the lower Oligocene by a disconformity with ~4 My missing. The lower Oligocene through middle Eocene has an average accumulation rate of ~8 m/My. This sequence is separated from the Turonian by a condensed interval containing several biostratigraphic units of the middle Paleocene. The lower Paleocene through upper Turonian is missing at a disconformity with a hiatus of at least 29 My. The middle Turonian through upper Albian has an average sediment accumulation rate of ~8 m/My.

Preliminary scientific assessment

Expedition 369 met the proposed science objectives and exceeded many during its investigation of the tectonic, paleoclimatic, and paleoceanographic history of the GAB and the MB. Sediment recovered from sites drilled in both regions will provide a new perspective on Earth's temperature variation at subpolar latitudes (60°–62°S) during the rise and fall of the mid-Cretaceous and early Eocene hothouse climates and ensuing paleoceanographic and biotic changes. The recovered sediment will also provide constraints on the timing of rifting and basin subsidence during the last phase of breakup among remnant Gondwana continents. The following is a discussion of how the objectives and additional discoveries were attained for each of the primary goals:

1. *Investigate the timing and causes for the rise and collapse of the Cretaceous hot greenhouse and how this climate mode affected the climate-ocean system and oceanic biota.*

Recovery of Cretaceous sediments that yielded foraminifers showing minimal diagenetic alteration was a major goal of Expedition 369 because these samples are essential for reliable Cretaceous climate reconstructions. We achieved this objective at Sites U1512–U1514, and U1516 (Figures **F9**, **F10**, **F11**, **F12**). The sequence that will yield the most continuous Cretaceous climate record ranges from the middle Albian through the early Campanian (~28 My) at Site U1513, adjacent to where Site 258 was drilled with only 22% Cretaceous sediment recovery (Luyendyk and Davies, 1974). Importantly, analysis of Cenomanian sediments yielding good microfossil preservation at Sites U1513, U1514, and U1516 will fill a critical temporal gap in the climate record at southern high latitudes. Moreover, good core recovery and microfossil preservation in portions of the Santonian–Turonian at Site U1512, Coniacian–Turonian and late Albian at Sites U1513 and U1514, and most of the Santonian–early Campanian at Site U1513 will significantly improve reconstructions of the climatic and oceanographic changes that occurred across the rise and fall of the hot Cretaceous greenhouse climate.

2. *Determine the relative roles of productivity, ocean temperature, and ocean circulation at high southern latitudes during Cretaceous OAEs.*

One of the most important goals of Expedition 369 was to obtain stratigraphically complete and well-preserved sediment records spanning OAE 2 (~93.8 Ma; Meyers et al., 2012) and OAE 1d (~100.2 Ma; Erbacher and Thurow, 1997; Bréhéret, 1988, 1997; Leckie et al., 2002). These short-lived (<1 My) episodes of enhanced deposition of organic carbon are associated with carbon isotope excursions and high rates of species turnover (Jenkyns, 1980, 2010; Arthur et al., 1988; Leckie et al., 2002; Jenkyns et al., 2012, 2017). The sediment records cored at Sites U1513, U1514, and U1516 exceeded our expectations for this objective. Complete and well-preserved microfossil assemblages were recovered from above, below, and within the OAE 2 and 1d intervals, together with laminated black shale beds. Some authors have suggested that OAE 2, which spans the C/T boundary (~94 Ma), was triggered by CO_2 outgassing during a widespread pulse of volcanism (Turgeon and Creaser, 2008; Du Vivier et al., 2014). The 97% composite recovery across OAE 2 in Holes U1513A and U1513D and 100% recovery in Holes U1516A and U1516C provide a unique opportunity to study this event in greater detail than any OAE 2 sequence in the world because of the abundance and good preservation of calcareous microfossils and organic biomarkers across the interval. Cores from across this interval at both sites include multiple black shale intervals with high TOC content (Figure **F11**). Osmium isotope measurements through the cored sequence will determine the timing of eruptions prior to, during, and after the event. Oxygen isotope analyses of well-preserved benthic and planktonic foraminifers should determine for the first time whether oceanic warming was triggered by a volcanic event and whether predicted cooling followed the burial of organic carbon during the peak of the OAE (Jenkyns et al.,

2017). Measurement of additional chemical proxies and study of the microfossil assemblages for both OAEs will characterize changes in carbon chemistry, nutrient flux, types and amount of organic carbon burial, and changes in microfossil assemblages. Results from study of the OAE intervals cored at Sites U1513–U1514 and U1516 will provide a significant advance in our understanding of the cause and effects of these global anoxic events. A final additional bonus was the recovery of the relatively little studied mid-Cenomanian event at Sites U1513 and U1516.

3. *Identify the main source regions for deep-water and intermediate water masses in the southeast Indian Ocean and how these changed during Gondwana breakup.*

Several intervals cored during Expedition 369 will be investigated using εNd to trace sources and circulation patterns of deep-water masses (and thus changing connections between basins), as well as local weathering inputs and potential global influences such as hydrothermal input from large igneous province volcanism. For the Cenomanian in general and the OAE 2 interval in particular, εNd patterns obtained from sediments cored at Sites U1513 and U1516 will provide a geographically distant test between competing volcanic and circulation models developed for the North Atlantic. Integration of deep circulation among basins and the increasing importance of the Southern Ocean as a deep-water source can be temporally constrained by comparing εNd values and trends in the MB cores to values documented elsewhere. Finally, the timing and regional importance of the opening of the Tasman Gateway and the evolution of Antarctic circulation patterns across the Eocene/Oligocene boundary can be determined from εNd values obtained from sediment cores at Site U1514 on the northern MB.

4. *Characterize how oceanographic conditions changed at the MB during the Cenozoic opening of the Tasman Passage and restriction of the Indonesian Gateway.*

The opening of the Tasman Passage and restriction of the Indonesian Passage were major factors that influenced the evolution of global climate during the Cenozoic, and both oceanic gateway changes profoundly affected the climate of Australia and Antarctica. The Eocene opening of the Drake Passage and the Tasman Gateway led to development of the cold ACC that isolated Antarctica from warm equatorial currents, resulting in the buildup of a continental ice sheet in Antarctica (Bijl et al., 2013; Scher et al., 2006). Northward movement of Australia toward equatorial waters during the Miocene caused substantial reorganization of ocean current pathways in the Indian Ocean and major shifts in the climate of Australia (Gallagher et al., 2017; Groeneveld et al., 2017). Continued northward movement restricted current circulation across the Indonesian Gateway during the Pliocene, which then reduced the influence of the warm-water Indonesian Throughflow in the Indian Ocean and initiated the arid climate that characterizes modern western Australia (Christensen et al. 2017).

Because of the mid-latitude location, Cenozoic sedimentation in the MB has been particularly sensitive to northern and southern movements of Antarctic waters and changes in oceanic gateway passages that connect the western equatorial Pacific Ocean with the Indian Ocean. Study of Eocene deposits recovered at Sites U1514 and U1516 will further our understanding of the oceanographic and climatic consequences of the opening of the Tasman Passage. High-resolution studies of Miocene and Pliocene sediments recovered from Sites U1513, U1415 and U1516 will establish the timing, magnitude, and rates of climate and ocean circulation changes that affected the Australian continent and the southeast Indian Ocean region as the seaway between Australia and Antarctica widened and deepened and the Indonesian Passage became more restricted.

5. *Resolve questions on the volcanic and sedimentary origins of the basin and provide vital stratigraphic control on the age and nature of the prebreakup succession.*

Sampling the prebreakup sediments was achieved at Site U1515. The margin-wide unconformity was crossed at 364 m CSF-A, and coring sampled a series of carbon-rich claystones interspersed with poorly cemented sandstone in a fault-bounded segment of the eastern MB. These claystones are believed to be of Early Jurassic age deposited during the early stages of rifting within Gondwana, which was undergoing a period of thermal subsidence following an earlier Permian rifting event (Bradshaw et al., 2003). Tilting of these sediments is indicative of a later stage of rifting and fault reactivation in the mid- to Late Jurassic.

Our deepest hole (U1513E) cored ~84 m of volcanic material and recovered ~54 m of material. Onboard analysis identified separate extrusive flow sequences intercalated with sedimentary breccia beds that were later intruded by a younger diabase dike. The older extrusive volcanics appear to be a mix of subaerial and marine flows, which suggests they were deposited close to sea level. Isotopic dating of the volcanics was not possible on board, although stratigraphic relations mean that the extrusive flows are older than the overlaying mid-Valanginian sediments as dated by magnetostratigraphy. Volcanic activity, as evidenced from the intersecting seismic profiles as either isolated bright reflectors that are interpreted as sills or as volcanic cones, appears to be present through lithostratigraphic Unit V, which is dated as Valanginian to Barremian. Although the basalt sequences are highly altered, we anticipate that enough material has been collected for Ar/Ar analysis to at least date some of the flows and dike. Results will be compared with a recent compilation of basalt samples from both nearby dredge and onland sampling of the Bunbury basalt (Direen et al., 2017; Olierook et al., 2016).

All Expedition 369 sites contribute to significantly improving the stratigraphic control of the regional reflection seismic data. Site U1512 recalibrates the current seismic interpretation and hence the role of the Wallaroo Fault System as an active fault synchronous with the initial phase of seafloor spreading between Antarctica and Australia. Sediments cored at sites around the MB enable dating of key stratigraphic units that record the rifting of both India and Antarctica from Australia that can be correlated to the regional seismic reflection data. Erosional hiatuses and faults in the sedimentary succession can now be dated and linked with episodes of uplift, erosion, and subsidence, which in turn can be linked to the wider tectonic and thermal histories of this margin.

Operations

Port call and initial transit to Site U1512

Expedition 369 officially began at 0754 h (UTC + 11 h) on 26 September 2017 with the first line ashore at Macquarie Wharf, Berth 4, in Hobart, Australia. The ship cleared immigration and customs, and Expedition 369 technical staff, the Expedition Project Manager, and the Co-Chief Scientists boarded the ship at 0930 h. The remainder of the science party boarded the vessel on 27 September, and public relations activities were conducted on 28 and 29 September. During the port call, the loading of drilling equipment, expedition stores, and food was completed, and installation of a

spare wireline logging cable was concluded. The ship left Hobart with the last line released at 0710 h on 30 September and began making its way to Site U1512. The 1425 nmi sea voyage ended at 0530 h (UTC + 8 h) on 7 October.

Site U1512

Site U1512 (Table **T1**) consisted of a single hole (U1512A) that was cored with the RCB system. The original plan was to advance to 570 m drilling depth below seafloor (DSF); however, it became apparent during coring operations that the Late Cretaceous sedimentary section was very expanded. Following revisions to coring depth estimates and Environmental Protection and Safety Panel approval, the hole was deepened to 700 m DSF. Coring operations and conditions were excellent although the hole deviated ~26° from vertical through what was fairly uniform lithology. After coring operations were completed, one downhole logging run was completed along the entire open borehole with the modified triple combo tool string, which measured NGR, density, resistivity, and velocity. Logging operations and conditions were also excellent.

Overall, 7.7 days (7–14 October 2017) were spent at Site U1512. A total of 73 RCB cores were recorded for the site, penetrating to a total depth of 700.8 m DSF and recovering 631.86 m of core (90% recovery).

Site U1513

Site U1513 (Table **T1**) consisted of coring and logging operations at five holes and was visited on two separate occasions. All of the coring systems were used: both the APC and half-length APC (HLAPC) systems in Holes U1513A–U1513C, the XCB system in Hole U1513A, and the RCB system in Holes U1513D and U1513E. Coring extended to 292.5 m DSF in Hole U1513A and crossed one of the critical boundaries for the expedition (C/T boundary). In situ formation temperatures were attempted with the advanced piston corer temperature tool (APCT-3), but only one value was returned for Core 369-U1513A-5H because the tool was damaged. Hole U1513B was intended to fill in recovery gaps from the Neogene and uppermost Cretaceous section from Hole U1513A and was cored to 98.6 m DSF; all cores were oriented with either the Icefield MI-5 core orientation tool or the FlexIT tool. Hole U1513C cores were sectioned on the catwalk into 30 cm whole rounds for postexpedition analyses. Hole U1513D penetrated to 757.4 m DSF and accomplished the deep target of the expedition objectives by recovering basalt; Hole U1513E then extended the basalt penetration and recovery to 774 m DSF. Downhole logging runs were attempted in Holes U1513A, U1513D, and U1513E. After coring operations were completed in Hole U1513A, one downhole logging run was completed along the entire length of the open borehole (to 289.8 m WSF) with the modified triple combo tool string, and runs with it were also attempted in Holes U1513D (to 346 m WSF) and U1513E from 426 to 614 m WSF. One run with the traditional triple combo tool string was also performed from 119 to 610 m WSF in Hole U1513E. A seismic experiment and FMS runs were also conducted in Hole U1513E from 426 to 637 m WSF (VSI) and 426 to 611 m WSF (FMS).

Overall, 15.5 days (18 October–2 November and 20–25 November 2017) were spent at Site U1513. A total of 18 APC, 13 HLAPC, 35 XCB, and 81 RCB cores were recorded for the site, penetrating to a total depth of 774 m DSF. Of the 1137.8 m cored, we recovered 777.07 m of material (80.8%).

Site U1514

Site U1514 (Table **T1**) consisted of coring and logging operations in three holes. All four of the coring systems were used. The piston coring (APC and HLAPC) and XCB systems were used in Hole U1514A, Hole U1514B was cored with the APC system only, and the RCB system was used in Hole U1514C. Hole U1514A extended to 255.6 m DSF, at which point the XCB was unable to penetrate deeper. All cores recovered with the APC system in Hole U1514A were oriented with either the Icefield MI-5 core orientation tool or FlexIT tool. Cores recovered from Hole U1514B were completely sectioned on the catwalk into 30 cm whole-round sections for postexpedition analyses. Hole U1514C penetrated to 516.8 m DSF and was successfully logged with the modified triple combo tool string.

Overall, 7.4 days (2–9 November 2017) were spent at Site U1514. A total of 21 APC, 5 HLAPC, 7 XCB, and 34 RCB cores were recorded for the site, penetrating to a total depth of 516.8 m DSF. Of the 591.9 m cored, 518.12 m of material was recovered (87.5%).

Site U1515

Operations at Site U1515 (Table **T1**) consisted of coring a single hole (U1515A) with the RCB system to 517.1 m DSF. The original plan for this site included coring three holes and a full suite of wireline logging runs. However, hole conditions were generally poor, which precluded logging, and core recovery was low, thus shortening the time spent at this site.

Overall, 55 RCB cores were recovered with 93.62 m recovered from the 517.1 m cored (18.1%). The total time on Site U1515 was 3.6 days (10–13 November 2017).

Site U1516

Four holes were cored at Site U1516. Hole U1516A was cored with the APC and HLAPC systems to 223.6 m DSF. All cores recovered with the APC system in Hole U1516A (Cores 1H through 20H) were oriented with the Icefield MI-5 core orientation tool or FlexIT tool. Successful in situ formation temperature measurements were made with the APCT-3 in Cores 369-U1516-3H, 5H, 7H, and 17H. Hole U1516B was cored with the APC system to ~15 m; all of the material was immediately sectioned on the catwalk in 30 cm whole rounds for postexpedition analyses. Hole U1516C, which was drilled without coring to 196 m DSF, was then cored with the RCB system to 541.6 m DSF. Hole U1516D aimed to recover an additional copy of the C/T boundary. It was drilled without coring to 458 m DSF and then cored with the RCB system to 477.6 m DSF, recovering four cores.

In total, 476.99 m was recovered from 605.0 m cored (78.8%). We recovered 206.57 m from 197.5 m cored (104.6%) with the APC system and recovered 43.55 m from 42.3 m (103%) and 226.87 m from 365.2 m (62.1%) cored with the RCB system. We spent 5.9 days at Site U1516. After Site U1516 was completed, we returned to Site U1513.

Transit to Fremantle, Australia

At 0525 h on 25 November 2017, the ship was underway to Fremantle, Australia. Expedition 369 ended at 0700 h on 26 November.

Education, outreach, and media

Three education and outreach personnel participated in Expedition 369: a museum educator from the US, a videographer from Brazil, and a photojournalist from the United Kingdom.

Live broadcasts

During this expedition, 3 museums, 23 schools, and 8 universities participated in live ship-to-shore broadcasts (Table **T2**). Overall, institutions from nine different countries participated (Brazil, China, France, Germany, Japan, Morocco, Republic of Korea, the United Kingdom, and the US) and from nine different states in the US (California, Florida, Louisiana, Michigan, Missouri, Nebraska, New York, Texas, and Washington, DC). We reached approximately 1514 people through the broadcasts.

Survey feedback

As part of the feedback process, we sent a survey to every group that participated in a broadcast. Out of 44 broadcasts, 19 participating groups filled out a survey.

According to the survey results,

- The average rating for the participants' experience was 4.71 out of 5,
- 100% of participants who completed the survey said they received the opportunity to ask questions,
- 92% of participants felt that the objectives of the expedition were clearly explained,
- Participants gave an average score of 4.32 out of 5 in regard to whether they felt the information was presented at a level appropriate to the age of their group,
- 85% of participants felt that they learned more about science content,
- 100% of participants felt that they learned more about the science process,
- 76% of participants felt that they learned more about careers in science, and
- The average score for participants who felt that the broadcast met their expectations was 4.24 out of 5.

Anecdotes from participants about broadcasts

- "[These broadcasts are a] quick and easy way to explore science careers and real-life applications."
- "[These broadcasts are] very important for the young scientists and the international community."
- "Our students appreciated this opportunity very much."
- "Thank you very much for the broadcast. [The students] enjoyed it a lot, and the explanation of the scientists was clear and very interesting."
- "It was a very good and unique experience for everybody here to "be" on board a science ship off the coast of Australia!"
- "We would like to participate more often."
- "I loved that the tour included the both the chemistry lab and core lab. Tours in the past have only focused on the core lab. The diversity was great, and better represented the vessel operations."
- "It was engaging for the students, showed them how scientists figured out the things we're learning in class, showed them that scientists are still figuring out new things, and that there are careers in geoscience (and science in general)."

Education projects completed at sea

- Thirteen articles about Expedition 369 written in Portuguese and published on three Brazilian web portals: Jornal da UNICAMP, Portal Capes, and SBPC.
- Two podcasts produced in Portuguese for the JR Soundcloud channel.
- Blogs about the expedition by one of the scientists, facilitated by one of the Education and Outreach officers and using her photos, published on The Geological Society of London and the Traveling Geologist websites.
- Photographic documentation of the expedition, which will be shared on the National Geographic Voices Blog.
- Visual and audio interviews with scientists.
- Postcards from Scientists series featured on the JR Blog and social media.
- Education packet with info sheet and videos for the Geological Society of London to share with United Kingdom schools and on social media.
- Microfossils embroidered onto fabric as examples for a resource packet that gives instructions and templates for interested participants to make their own.
- Educational packet containing a story about scientific phenomena and concepts portrayed as wrestlers with several wrestling masks.
- Two series of coloring pages, one exploring life aboard the JR and one helping to explain how scientists study cores.
- A photo posted on Instagram as part of the Oz Rock Stock Take contest that won a prize from the Australian Geological Council.
- A newsletter about the highlights of Expedition 369 distributed to all the schools that participated in broadcasts.
- A book club series featured on the JR Blog highlighting scientists and other expedition members.

Media impact

The education and outreach team worked with various media outlets in Brazil, the United Kingdom, and the US, and the expedition was covered by other media sources in several other countries.

BBC Earth featured several photos of Expedition 369 on their Instagram account and Twitter account. We conducted two TV live interviews with BBC News and one with BBC Radio, as well as one live radio interview with the Australia Broadcasting Corporation. In Brazil, a 10 min prerecorded story was produced by BAND Cidades channel (**https://youtu.be/L5WCA19KOqA**).

Additional media coverage included a Reddit Ask Me Anything (AMA) session where several of the scientists on board assisted in fielding questions asked by the public. The questions and answers can be viewed at **https://www.reddit.com/r/science/comments/7b4g8u/science_ama_series_were_scientists_on_a_-ship_off/**. There were >1000 views of the session, with 196 people voting positively for the session (86% of the vote). More than 33 questions were asked and answered.

Smithsonian.com (**https://www.smithsonianmag.com**), which has a circulation of >6 million per month, commissioned three articles about the expedition for publication soon after the end of the expedition.

BBC Future, which has global circulation through BBC Worldwide, commissioned two short (3–4 min) films about the expedition that will likely come out in early 2018.

More appearances (Brazilian outreach)

- **http://confap.org.br/news/conheca-o-novo-espaco-de-divulgacao-das-ciencias-do-mar**
- **http://portal.mec.gov.br/component/content/article?id=55151:estudantes-poderao-acompanhar-expedicao-cientifica-pela-internet**
- **http://www.paqtc.org.br/portal_novo/3versao/html_paqtc//detailArtigo.action;jsessionid=7161B1633C7960DD1015A5302187DBCB?localDetail=principal&idEncript=Xe1yci67wqw%3D**
- **http://www.correiobraziliense.com.br/app/noticia/eu-estudante/ensino_educacaobasica/2017/09/29/ensino_educacaobasica_interna,630182/estudantes-poderao-acompanhar-expedicao-cientifica-pela-internet.shtml**
- **http://www.capes.gov.br/diariodebordo/noticias/noticia/8576-agente-de-divulgacao-conta-primeiras-impressoes-sobre-expedicao-em-alto-mar**
- **http://www.unicamp.br/unicamp/ju/artigos/cristiane-delfina/sobre-expedicoes**
- **http://www.gestaouniversitaria.com.br/artigos/conheca-o-novo-espaco-de-divulgacao-das-ciencias-do-mar**
- **http://www.abruc.org.br/003/00301015.asp?ttCD_CHAVE=270350&btImprimir=SIM**
- **http://www.sinepenopr.com.br/artigos/boletim-sinepe-nopr-03-de-outubro-de-2017**
- **http://gestaouniversitaria.com.br/artigos/capes-tem-sala-de-interacao-na-14-semana-nacional-de-ciencia-e-tecnologia**

Social media

- +281 followers on Facebook (between 26 September and 23 November 2017) (Table **T3**)
- +157 followers on Instagram (between 26 September and 23 November 2017)
- +124 followers and +195.0K impressions on Twitter (between 26 September and 23 November 2017)

The increase of organic (not attracted by paid ads) followers is the most targeted and hardest to achieve by social media content producers. These followers are real people willing to engage with the brand/institution. Because Facebook and Instagram have algorithms to increase their gains with paid advertisements, they will first show the paid content to the users. The numbers shown above are very high because we achieved only organic users. This is a sign that the content is attracting people, and they are important followers of the *JOIDES Resolution* community.

References

Ando, A., Huber, B.T., MacLeod, K.G., Ohta, T., and Khim, B.-K., 2009. Blake Nose stable isotopic evidence against the mid-Cenomanian glaciation hypothesis. *Geology*, 37(5):451–454. **https://doi.org/10.1130/G25580A.1**

Ando, A., Kakegawa, T., Takashima, R., and Saito, T., 2002. New perspective on Aptian carbon isotope stratigraphy: data from $\delta^{13}C$ records of terrestrial organic matter. *Geology*, 30(3):227–230. **https://doi.org/10.1130/0091-7613(2002)030<0227:NPOACI>2.0.CO;2**

Arthur, M.A., Dean, W.E., and Pratt, L.M., 1988. Geochemical and climatic effects of increased marine organic carbon burial at the Cenomanian/Turonian boundary. *Nature,* 335(6192):714–717. **https://doi.org/10.1038/335714a0**

Barrera, E., Savin, S.M., Thomas, E., and Jones, C.E., 1997. Evidence for thermohaline-circulation reversals controlled by sea- level change in the latest Cretaceous. *Geology,* 25(8):715–718. **https://doi.org/10.1130/0091-7613(1997)025<0715:EFTCRC>2.3.CO;2**

Barron, E.J., 1983. A warm, equable Cretaceous: the nature of the problem. *Earth-Science Reviews,* 19(4):305–338. **https://doi.org/10.1016/0012-8252(83)90001-6**

Bice, K.L., Huber, B.T., and Norris, R.D., 2003. Extreme polar warmth during the Cretaceous greenhouse? Paradox of the late Turonian $\delta^{18}O$ record at Deep Sea Drilling Project Site 511. *Paleoceanography,* 18(2):1031. **https://doi.org/10.1029/2002PA000848**

Bijl, P.K., Bendle, J.A.P., Bohaty, S.M., Pross, J., Schouten, S., Tauxe, L., Stickley, C.E., McKay, R.M., Röhl, U., Olney, M., Sluijs, A., Escutia, C., Brinkhuis, H., and Expedition 318 Scientists, 2013. Eocene cooling linked to early flow across the Tasmanian Gateway. *Proceedings of the National Academy of Sciences of the United States of America,* 110(24):9645–9650. **https://doi.org/10.1073/pnas.1220872110**

Borissova, I., 2002. *Geological Framework of the Naturaliste Plateau.* Geoscience Australia, 2002/20. **http://www.ga.gov.au/metadata-gateway/metadata/record/40535/**

Borissova, I., Bradshaw, B.E., Nicholson, C., Struckmeyer, H.I.M., and Payne, D., 2010. New exploration opportunities on the southwest Australian margin: deep-water frontier Mentelle Basin. *APPEA Journal,* 50:1–13.

Bornemann, A., Norris, R.D., Friedrich, O., Beckmann, B., Schouten, S., Sinninghe Damsté, J.S., Vogel, J., Hofmann, P., and Wagner, T., 2008. Isotopic evidence for glaciation during the Cretaceous supergreenhouse. *Science,* 319(5860):189–192. **https://doi.org/10.1126/science.1148777**

Borrelli, C., Cramer, B.S., and Katz, M.E., 2014. Bipolar Atlantic deepwater circulation in the middle-late Eocene: effects of Southern Ocean gateway openings. *Paleoceanography,* 29(4):308–327. **https://doi.org/10.1002/2012PA002444**

Bowman, V.C., Francis, J.E., Riding, J.B., Hunter, S.J., and Haywood, A.M., 2012. A latest Cretaceous to earliest Paleogene dinoflagellate cyst zonation from Antarctica, and implications for phytoprovincialism in the high southern latitudes. *Review of Palaeobotany and Palynology,* 171:40–56. **https://doi.org/10.1016/j.revpalbo.2011.11.004**

Bradshaw, B.E., Rollet, N., Totterdell, J.M., and Borissova, I., 2003. A revised structural framework for frontier basins on the southern and southwestern Australian continental margin. *Geoscience Australia,* 2003/03. **https://d28rz98at9flks.cloudfront.net/42056/Rec2003_003.pdf**

Cane, M.A., and Molnar, P., 2001. Closing of the Indonesian Seaway as a precursor to East African aridification around 3–4 million years ago. *Nature,* 411(6834):157–162. **https://doi.org/10.1038/35075500**

Clarke, L.J., and Jenkyns, H.C., 1999. New oxygen isotope evidence for long-term Cretaceous climatic change in the Southern Hemisphere. *Geology,* 27(8):699–702. **https://doi.org/10.1130/0091-7613(1999)027<0699:NOIEFL>2.3.CO;2**

Cramer, B.S., Toggweiler, J.R., Wright, J.D., Katz, M.E., and Miller, K.G., 2009. Ocean overturning since the Late Cretaceous: inferences from a new benthic foraminiferal isotope compilation. *Paleoceanography,* 24(4). **https://doi.org/10.1029/2008PA001683**

Direen, N.G., Cohen, B.E., Maas, R., Frey, F.A., Whittaker, J.M., Coffin, M.F., Meffre, S., Halpin, J.A., and Crawford, A.J., 2017. Naturaliste Plateau: constraints on the timing and evolution of the Kerguelen Large Igneous Province and its role in Gondwana breakup. *Australian Journal of Earth Sciences,* 64(7):851–869. **https://doi.org/10.1080/08120099.2017.1367326**

Direen, N.G., Stagg, H.M.J., Symonds, P.A., and Colwell, J.B., 2011. Dominant symmetry of a conjugate southern Australian and East Antarctic magma-poor rifted margin segment. *Geochemistry, Geophysics, Geosystems,* 12(2):Q02006. **https://doi.org/10.1029/2010GC003306**

Divakaran, P., and Brassington, G.B., 2011. Arterial ocean circulation of the southeast Indian Ocean. *Geophysical Research Letters,* 38(1):L01802. **https://doi.org/10.1029/2010GL045574**

Domingues, C.M., Maltrud, M.E., Wijffels, S.E., Church, J.A., and Tomczak, M., 2007. Simulated Lagrangian pathways between the Leeuwin Current System and the upper-ocean circulation of the southeast Indian Ocean.

Deep Sea Research Part II: Topical Studies in Oceanography, 54(8–10):797–817. **https://doi.org/10.1016/j.dsr2.2006.10.003**

Du Vivier, A.D.C., Selby, D., Sageman, B.B., Jarvis, I., Gröcke, D.R., and Voigt, S., 2014. Marine $^{187}Os/^{188}Os$ isotope stratigraphy reveals the interaction of volcanism and ocean circulation during oceanic anoxic Event 2. *Earth and Planetary Science Letters,* 389:23–33. **https://doi.org/10.1016/j.epsl.2013.12.024**

Erbacher, J., and Thurow, J., 1997. Influence of oceanic anoxic events on the evolution of mid-Cretaceous radiolaria in the North Atlantic and western Tethys. *Marine Micropaleontology,* 30(1–3):139–158. **https://doi.org/10.1016/S0377-8398(96)00023-0**

Frakes, L.A., Francis, J.E., and Syktus, J.I., 1992. *Climate Modes of the Phanerozoic:* Cambridge, United Kingdom (Cambridge University Press).

Friedrich, O., Schiebel, R., Wilson, P.A., Weldeab, S., Beer, C.J., Cooper, M.J., and Fiebig, J., 2012. Influence of test size, water depth, and ecology on Mg/Ca, Sr/Ca, $\delta^{18}O$ and $\delta^{13}C$ in nine modern species of planktic foraminifers. *Earth and Planetary Science Letters,* 319–320:133–145. **https://doi.org/10.1016/j.epsl.2011.12.002**

Gale, A.S., Hardenbol, J., Hathway, B., Kennedy, W.J., Young, J.R., and Phansalkar, V., 2002. Global correlation of Cenomanian (Upper Cretaceous) sequences: evidence for Milankovitch control on sea level. *Geology,* 30(4):291–294. **https://doi.org/10.1130/0091-7613(2002)030<0291:GCOCUC>2.0.CO;2**

Gallagher, S.J., Fulthorpe, C.S., Bogus, K., Auer, G., Baranwal, S., Castañeda, I.S., Christensen, B.A., De Vleeschouwer, D., Franco, D.R., Groeneveld, J., Gurnis, M., Haller, C., He, Y., Henderiks, J., Himmler, T., Ishiwa, T., Iwatani, H., Jatiningrum, R.S., Kominz, M.A., Korpanty, C.A., Lee, E.Y., Levin, E., Mamo, B.L., McGregor, H.V., McHugh, C.M., Petrick, B.F., Potts, D.C., Lari, A.R., Renema, W., Reuning, L., Takayanagi, H., and Zhang, W., 2017. Expedition 356 summary. *In* Gallagher, S.J., Fulthorpe, C.S., Bogus, K., and the Expedition 356 Scientists, *Indonesian Throughflow.* Proceedings of the International Ocean Discovery Program, 356: College Station, TX (International Ocean Discovery Program). **https://doi.org/10.14379/iodp.proc.356.101.2017**

Gibbons, A.D., Whittaker, J.M., and Müller, R.D., 2013. The breakup of East Gondwana: assimilating constraints from Cretaceous ocean basins around India into a best-fit tectonic model. *Journal of Geophysical Research: Solid Earth,* 118(3):808–822. **https://doi.org/10.1002/jgrb.50079**

Godfrey, J.S., 1996. The effect of the Indonesian throughflow on ocean circulation and heat exchange with the atmosphere: a review. *Journal of Geophysical Research: Oceans,* 101(C5):12217–12237. **https://doi.org/10.1029/95JC03860**

Gordon, A.L., 1986. Interocean exchange of thermocline water. *Journal of Geophysical Research: Oceans,* 91(C4):5037–5046. **https://doi.org/10.1029/JC091iC04p05037**

Gröcke, D.R., Hesselbo, S.P., and Jenkyns, H.C., 1999. Carbon-isotope composition of Lower Cretaceous fossil wood: ocean-atmosphere chemistry and relation to sea-level change. *Geology,* 27(2):155–158. **https://doi.org/10.1130/0091-7613(1999)027<0155:CICOLC>2.3.CO;2**

Groeneveld, J., Henderiks, J., Renema, W., McHugh, C.M., De Vleeschouwer, D., Christensen, B.A., Fulthorpe, C.S., et al., 2017. Australian shelf sediments reveal shifts in Miocene Southern Hemisphere westerlies. *Science Advances,* 3(5):e1602567. **https://doi.org/10.1126/sciadv.1602567**

Hay, W.W., 2008. Evolving ideas about the Cretaceous climate and ocean circulation. *Cretaceous Research,* 29(5–6):725–753. **https://doi.org/10.1016/j.cretres.2008.05.025**

Hay, W.W., DeConto, R.M., Wold, C.N., Wilson, K.M., Voigt, S., Schulz, M., Rossby Wold, A., Dullo, W.-C., Ronov, A.B., Balukhovsky, A.N., and Söding, E., 1999. Alternative global Cretaceous paleogeography. *In* Barrera, E., and Johnson, C.C. (Eds.), *Evolution of the Cretaceous Ocean-Climate System*. Special Paper - Geological Society of America, 332:1–47. **https://doi.org/10.1130/0-8137-2332-9.1**

Hollis, C.J., Taylor, K.W.R., Handley, L., Pancost, R.D., Huber, M., Creech, J.B., Hines, B.R., Crouch, E.M., Morgans, H.E.G., Crampton, J.S., Gibbs, S., Pearson, P.N., and Zachos, J.C., 2012. Early Paleogene temperature history of the Southwest Pacific Ocean: reconciling proxies and models. *Earth and Planetary Science Letters,* 349–350:53–66. **https://doi.org/10.1016/j.epsl.2012.06.024**

Huber, B.T., Hodell, D.A., and Hamilton, C.P., 1995. Mid- to Late Cretaceous climate of the southern high latitudes: stable isotopic evidence for minimal equator-to-pole thermal gradients. *Geological Society of America Bulletin,* 107(10):1164–1191. **https://doi.org/10.1130/0016-7606(1995)107<1164:MLCCOT>2.3.CO;2**

Huber, B.T., MacLeod, K.G., Gröcke, D.R., and Kucera, M., 2011. Paleotemperature and paleosalinity inferences and chemostratigraphy across the Aptian/Albian boundary in the subtropical North Atlantic. *Paleoceanography,* 26(4). **https://doi.org/10.1029/2011PA002178**

Huber, B.T., MacLeod, K.G., Watkins, D.K., and Coffin, M.F., submitted. The rise and fall of the Cretaceous hot greenhouse climate. *Global and Planetary Change.*

Huber, B.T., Norris, R.D., and MacLeod, K.G., 2002. Deep sea paleotemperature record of extreme warmth during the Cretaceous. *Geology,* 30(2):123–126. **https://doi.org/10.1130/0091-7613(2002)030<0123:DSPROE>2.0.CO;2**

Huber, M., Brinkhuis, H., Stickley, C.E., Döös, K., Sluijs, A., Warnaar, J., Schellenberg, S.A., and Williams, G.L., 2004. Eocene circulation of the Southern Ocean: was Antarctica kept warm by subtropical waters? *Paleoceanography,* 19(4):PA4026. **https://doi.org/10.1029/2004PA001014**

Jahren, A.H., Arens, N.C., Sarmiento, G., Guerrero, J., and Amundson, R., 2001. Terrestrial record of methane hydrate dissociation in the Early Cretaceous. *Geology,* 29(2):159–162. **https://doi.org/10.1130/0091-7613(2001)029<0159:TROMHD>2.0.CO;2**

Jarvis, I., Gale, A.S., Jenkyns, H.C., and Pearce, M.A., 2006. Secular variation in Late Cretaceous carbon isotopes: a new $\delta^{13}C$ carbonate reference curve for the Cenomanian–Campanian (99.6–70.6 Ma). *Geological Magazine,* 143(5):561–608. **https://doi.org/10.1017/S0016756806002421**

Jenkyns, H.C., Dickson, A.J., Ruhl, M., and van den Boorn, S.H.J.M., 2017. Basalt-seawater interaction, the Plenus Cold Event, enhanced weathering and geochemical change: deconstructing oceanic anoxic Event 2 (Cenomanian–Turonian, Late Cretaceous). *Sedimentology,* 64(1):16–43. **https://doi.org/10.1111/sed.12305**

Jenkyns, H.C., 1980. Cretaceous anoxic events: from continents to oceans. *Journal of the Geological Society,* 137(2):171–188. **https://doi.org/10.1144/gsjgs.137.2.0171**

Jenkyns, H.C., 2010. Geochemistry of oceanic anoxic events. *Geochemistry, Geophysics, Geosystems,* 11(3):Q03004. **https://doi.org/10.1029/2009GC002788**

Jenkyns, H.C., Schouten-Huibers, L., Schouten, S., and Sinninghe Damsté, J.S., 2012. Warm Middle Jurassic–Early Cretaceous high-latitude sea-surface temperatures from the Southern Ocean. *Climate of the Past,* 8(1):215–226. **https://doi.org/10.5194/cp-8-215-2012**

Jiménez Berrocoso, Á., MacLeod, K.G., Huber, B.T., Lees, J.A., Wendler, I., Bown, P.R., Mweneinda, A.K., Isaza Londoño, C., and Singano, J.M., 2010. Lithostratigraphy, biostratigraphy and chemostratigraphy of Upper Cretaceous sediments from southern Tanzania: Tanzania Drilling Project Sites 21–26. *Journal of African Earth Sciences,* 57(1–2):47–69. **https://doi.org/10.1016/j.jafrearsci.2009.07.010**

Jung, C., Voigt, S., Friedrich, O., Koch, M.C., and Frank, M., 2013. Campanian–Maastrichtian ocean circulation in the tropical Pacific. *Paleoceanography,* 28(3):562–573. **https://doi.org/10.1002/palo.20051**

Karas, C., Nürnberg, D., Gupta, A.K., Tiedemann, R., Mohan, K., and Bickert, T., 2009. Mid-Pliocene climate change amplified by a switch in Indonesian subsurface throughflow. *Nature Geoscience,* 2(6):434–438. **https://doi.org/10.1038/ngeo520**

Kuhnt, W., Holbourn, A., Hall, R., Zuvela, M., and Käse, R., 2004. Neogene history of the Indonesian Throughflow. *In* Clift, P., Wang, P., Kuhnt, W., and Hayes, D. (Eds.), *Continent-Ocean Interactions within East Asian Marginal Seas.* Geophysical Monograph, 149:299–320. **https://doi.org/10.1029/149GM16**

Leckie, R.M., Bralower, T.J., and Cashman, R., 2002. Oceanic anoxic events and plankton evolution: biotic response to tectonic forcing during the mid-Cretaceous. *Paleoceanography,* 17(3):1041. **https://doi.org/10.1029/2001PA000623**

Lee, T., Fukumori, I., Menemenlis, D., Xing, Z., and Fu, L.-L., 2002. Effects of the Indonesian throughflow on the Pacific and Indian Oceans. *Journal of Physical Oceanography,* 32(5):1404–1429. **https://doi.org/10.1175/1520-0485(2002)032<1404:EOTITO>2.0.CO;2**

Lumpkin, R., and Speer, K., 2007. Global ocean meridional overturning. *Journal of Physical Oceanography,* 37(10):2550–2562. **https://doi.org/10.1175/JPO3130.1**

MacLeod, K.G., Huber, B.T., Jiménez Berrocoso, Á., and Wendler, I., 2013. A stable and hot Turonian without glacial $\delta^{18}O$ excursions is indicated by exquisitely preserved Tanzanian foraminifera. *Geology,* 41(10):1083–1086. **https://doi.org/10.1130/G34510.1**

MacLeod, K.G., Londoño, C.I., Martin, E.E., Jiménez Berrocoso, Á., and Basak, C., 2011. Changes in North Atlantic circulation at the end of the Cretaceous greenhouse interval. *Nature Geoscience,* 4(11):779–782. **https://doi.org/10.1038/ngeo1284**

Maloney, D., Sargent, C., Direen, N.G., Hobbs, R.W., and Gröcke, D.R., 2011. Re-evaluation of the Mentelle Basin, a polyphase rifted margin basin, offshore southwest Australia: new insights from integrated regional seismic datasets. *Solid Earth,* 2(2):107–123. **https://doi.org/10.5194/se-2-107-2011**

Maritati, A., Aitken, A.R.A., Young, D.A., Roberts, J.L., Blankenship, D.D., and Siegert, M.J., 2016. The tectonic development and erosion of the Knox Subglacial Sedimentary Basin, East Antarctica. *Geophysical Research Letters,* 43(20):10,728–10,737. **https://doi.org/10.1002/2016GL071063**

Martin, E.E., and Scher, H.D., 2004. Preservation of seawater Sr and Nd isotopes in fossil fish teeth: bad news and good news. *Earth and Planetary Science Letters,* 220(1–2):25–39. **https://doi.org/10.1016/S0012-821X(04)00030-5**

Martin, E.E., MacLeod, K.G., Jiménez Berrocoso, A., and Bourbon, E., 2012. Water mass circulation on Demerara Rise during the Late Cretaceous based on Nd isotopes. *Earth and Planetary Science Letters,* 327–328:111–120. **https://doi.org/10.1016/j.epsl.2012.01.037**

McCartney, M.S., and Donohue, K.A., 2007. A deep cyclonic gyre in the Australian–Antarctic Basin. *Progress in Oceanography,* 75(4):675–750. **https://doi.org/10.1016/j.pocean.2007.02.008**

Meuleners, M.J., Pattiaratchi, C.B., and Ivey, G.N., 2007. Numerical modelling of the mean flow characteristics of the Leeuwin Current System. *Deep Sea Research Part II: Topical Studies in Oceanography,* 54(8–10):837–858. **https://doi.org/10.1016/j.dsr2.2007.02.003**

Meyers, S.R., Siewert, S.E., Singer, B.S., Sageman, B.B., Condon, D.J., Obradovich, J.D., Jicha, B.R., and Sawyer, D.A., 2012. Intercalibration of radioisotopic and astrochronologic time scales for the Cenomanian–Turonian boundary interval, Western Interior Basin, USA. *Geology,* 40(1):7–10. **http://dx.doi.org/10.1130/G32261.1**

Middleton, J.F., and Cirano, M., 2002. A northern boundary current along Australia's southern shelves: the Flinders Current. *Journal of Geophysical Research: Oceans,* 107(C9):3129. **https://doi.org/10.1029/2000JC000701**

Miller, K.G., Barrera, E., Olsson, R.K., Sugarman, P. J., and Savin, S.M., 1999. Does ice drive early Maastrichtian eustasy? *Geology,* 27(9):783–786. **https://doi.org/10.1130/0091-7613(1999)027<0783:DIDEME>2.3.CO;2**

Miller, K.G., Kominz, M.A., Browning, J.V., Wright, J.D., Mountain, G.S., Katz, M.E., Sugarman, P.J., Cramer, B.S., Christie-Blick, N., and Pekar, S.F., 2005. The Phanerozoic record of global sea-level change. *Science,* 310(5752):1293–1298. **https://doi.org/10.1126/science.1116412**

Moiroud M., Pucéat, E., Donnadieu, Y., Bayon, G., Moriya, K., Deconinck, J.-F., and Boyet, M., 2013. Evolution of the neodymium isotopic signature of neritic seawater on a northwestern Pacific margin: new constrains on possible end-members for the composition of deep-water masses in the Late Cretaceous ocean. *Chemical Geology,* 356:160–170. **https://doi.org/10.1016/j.chemgeo.2013.08.008**

Moriya, K., Wilson, P.A., Friedrich, O., Erbacher, J., and Kawahata, H., 2007. Testing for ice sheets during the mid-Cretaceous greenhouse using glassy foraminiferal calcite from the mid-Cenomanian tropics on Demerara rise. *Geology,* 35(7):615–618. **https://doi.org/10.1130/G23589A.1**

Müller, R.D., Gaina, C., and Clarke, S., 2000. Seafloor spreading around Australia. *In* Veevers, J.J. (Ed.), *Billion-Year Earth History of Australia and Neighbours in Gondwanaland*: Sydney (GEMOC Press), 18–28.Murphy, D.P., and Thomas, D.J., 2012. Cretaceous deep-water formation in the Indian sector of the Southern Ocean. *Paleoceanography,* 27(1). **https://doi.org/10.1029/2011PA002198**

O'Brien, C.L., Robinson, S.A., Pancost, R.D., Sinninghe Damsté, J.S., Schoulten, S., Lunt, D.J., Alsenz, H., Bornemann, A., Bottini, C., Brassell, S.C., Farnsworth, A., Forster, A., Huber, B.T., Inglis, G.N., Jenkyns, H.C., Linnert, C., Littler, K., Markwick, P., McAnena, A., Mutterlose, J., Naafs, B.D.A., Püttmann, W., Sluijs, A., van Helmond, N.A.G.M., Vellekoop, J., Wagner, T., and Wrobel, N.E., 2017. Cretaceous sea-surface temperature evolution: constraints from TEX_{86} and planktonic foraminiferal oxygen isotopes. *Earth-Science Reviews,* 172:224–247. **https://doi.org/10.1016/j.earscirev.2017.07.012**

Olierook, H.K.H., Jourdan, F., Merle, R.E., Timms, N.E., Kusznir, N., and Muhling, J.R., 2016. Bunbury basalt: Gondwana breakup products or earliest vestiges of the Kerguelen mantle plume? *Earth and Planetary Science Letters,* 440:20–32. **https://doi.org/10.1016/j.epsl.2016.02.008**

Pattiaratchi, C., 2006. Surface and sub-surface circulation and water masses off Western Australia. *Bulletin of the Australian Meteorological and Oceanographic Society,* 19:95–104.

Petkovic, P., 1975. Naturaliste Plateau. *In* Veevers, J.J. (Ed.), *Deep Sea Drilling in Australasian Waters:* North Ryde, N.S.W., Australia (Macquarie University), 24–25.

Ridgway, K.R., and Dunn, J.R., 2007. Observational evidence for a Southern Hemisphere oceanic supergyre. *Geophysical Research Letters,* 34(13):L13612. **https://doi.org/10.1029/2007GL030392**

Robinson, S.A., Murphy, D.P., Vance, D., and Thomas, D.J., 2010. Formation of "Southern Component Water" in the Late Cretaceous: evidence from Nd-isotopes. *Geology,* 38(10):871–874. **https://doi.org/10.1130/G31165.1**

Robinson, S.A., and Vance, D., 2012. Widespread and synchronous change in deep-ocean circulation in the North and South Atlantic during the Late Cretaceous. *Paleoceanography,* 27(1):PA1102. **https://doi.org/10.1029/2011PA002240**

Scher, H.D., and Martin, E.E., 2006. Timing and climatic consequences of the opening of Drake Passage. *Science,* 312(5772):428–430. **https://doi.org/10.1126/science.1120044**

Schlanger, S.O., and Jenkyns, H.C., 1976. Cretaceous oceanic anoxic events: causes and consequences. *Geologie en Mijnbouw,* 55:179–184.

Sloyan, B.M., 2006. Antarctic bottom and lower circumpolar deep water circulation in the eastern Indian Ocean. *Journal of Geophysical Research: Oceans,* 111(C2):C02006. **https://doi.org/10.1029/2005JC003011**

Speich, S., Blanke, B., and Cai, W., 2007. Atlantic meridional overturning circulation and the Southern Hemisphere supergyre. *Geophysical Research Letters,* 34(23):L23614. **https://doi.org/10.1029/2007GL031583**

Speich, S., Blanke, B., de Vries, P., Drijfhout, S., Döös, K., Ganachaud, A., and Marsh, R., 2002. Tasman leakage: a new route in the global ocean conveyor belt. *Geophysical Research Letters,* 29(10):55-1–55-4. **https://doi.org/10.1029/2001GL014586**

Stoll, H.M., and Schrag, D.P., 2000. High-resolution stable isotope records from the upper Cretaceous of Italy and Spain: glacial episodes in a greenhouse planet? *Geological Society of America Bulletin,* 112(2):308–319. **https://doi.org/10.1130/0016-7606(2000)112<0308:HRSIRF>2.3.CO;2**

Totterdell, J.M., Blevin, J.E., Struckmeyer, H.I.M., Bradshaw, B.E., Colwell, J.B., and Kennard, J.M., 2000. A new stratigraphic framework for the Great Australian Bight: starting with a clean slate. *APPEA Journal,* 40:95–117.

Totterdell, J.M., Struckmeyer, H.I.M., Boreham, C.J., Mitchell, C.H., Monteil, E., and Bradshaw, B.E., 2008. Mid–Late Cretaceous organic-rich rocks from the eastern Bight Basin: implications for prospectivity. *In* Blevin, J.E., Bradshaw, B.E., and Uruski, C. (Eds.), *Eastern Australasian Basins Symposium III.* Petroleum Exploration Society of Australia Special Publication, 137–158.

Turgeon, S.C., and Creaser, R.A., 2008. Cretaceous oceanic anoxic Event 2 triggered by a massive magmatic episode. *Nature,* 454(7202):323–326. **https://doi.org/10.1038/nature07076**

van Sebille, E., England, M.H., Zika, J.D., and Sloyan, B.M., 2012. Tasman leakage in a fine-resolution ocean model. *Geophysical Research Letters,* 39(6):L06601. **https://doi.org/10.1029/2012GL051004**

Veevers, J.J., 2006. Updated Gondwana (Permian–Cretaceous) earth history of Australia. *Gondwana Research*, 9(3):231–260. **https://doi.org/10.1016/j.gr.2005.11.005**

Voigt, S., Jung, C., Friedrich, O., Frank, M., Teschner, C., and Hoffmann, J., 2013. Tectonically restricted deep-ocean circulation at the end of the Cretaceous greenhouse. *Earth and Planetary Science Letters,* 369–370:169–177. **https://doi.org/10.1016/j.epsl.2013.03.019**

Waite, A.M., Thompson, P.A., Pesant, S., Feng, M., Beckley, L.E., Domingues, C.M., Gaughan, D., Hanson, C.E., Holl, C.M., Koslow, T., Meuleners, M., Montoya, J.P., Moore, T., Muhling, B.A., Paterson, H., Rennie, S., Strzelecki, J., and Twomey, L., 2007. The Leeuwin Current and its eddies: an introductory overview. *Deep Sea Research Part II: Topical Studies in Oceanography,* 54(8–10):789–796. **https://doi.org/10.1016/j.dsr2.2006.12.008**

White, L.T., Gibson, G.M., and Lister, G.S., 2013. A reassessment of paleogeographic reconstructions of eastern Gondwana: bringing geology back into the equation. *Gondwana Research,* 24(3–4):984–998. **https://doi.org/10.1016/j.gr.2013.06.009**

Zheng, X.-Y., Jenkyns, H.C., Gale, A.S., Ward, D.J., and Henderson, G.M., 2013. Changing ocean circulation and hydrothermal inputs during oceanic anoxic Event 2 (Cenomanian–Turonian): evidence from Nd-isotopes in the European shelf sea. *Earth and Planetary Science Letters,* 375:338–348. **https://doi.org/10.1016/j.epsl.2013.05.053**

Table T1. Expedition 369 hole summary.

Hole	Latitude	Longitude	Water depth (m)	Penetration DSF (m)	Interval cored (m)	Core recovered (m)	Recovery (%)	Drilled interval (m)	Drilled interval (*N*)	Total cores (*N*)
U1512A	34°01.6406′S	127°57.7605′E	3070.87	700.8	700.8	631.86	90.16		0	73
U1513A	33°47.6084′S	112°29.1338′E	2789.19	292.5	292.5	170.60	58.32		0	50
U1513B	33°47.6087′S	112°29.1471′E	2787.22	98.6	98.6	102.06	103.51		0	14
U1513C	33°47.6190′S	112°29.1468′E	2788.32	17.1	17.1	17.37	101.58		0	2
U1513D	33°47.6196′S	112°29.1339′E	2788.92	757.4	662.4	437.05	65.98	95.0	1	74
U1513E	33°47.6190′S	112°29.1204′E	2788.62	774.0	67.2	49.99	74.39	706.8	2	7
U1514A	33°7.2327′S	113°5.4672′E	3838.20	255.6	255.6	255.20	99.84		0	31
U1514B	33°7.2335′S	113°5.4798′E	3838.72	15.1	15.1	15.45	102.32		0	2
U1514C	33°7.2443′S	113°5.4799′E	3838.79	516.8	321.2	247.48	77.05	195.6	1	34
U1515A	33°16.1890′S	114°19.3666′E	849.70	517.1	517.1	93.62	18.10		0	55
U1516A	34°20.9169′S	112°47.9553′E	2676.46	223.6	223.6	233.26	104.32		0	29
U1516B	34°20.9175′S	112°47.9684′E	2676.42	16.2	16.2	16.81	103.77		0	2
U1516C	34°20.9272′S	112°47.9711′E	2676.62	541.6	345.6	208.32	60.28	196.0	1	40
U1516D	34°20.9277′S	112°47.9573′E	2676.62	477.6	19.6	18.55	94.64	458.0	1	4
			Totals:	5204.0	3552.6	2497.62		1651.4	6	417

Hole	Latitude	Longitude	APC cores (*N*)	HLAPC cores (*N*)	XCB cores (*N*)	RCB cores (*N*)	Date started (2017)	Time started (h UTC)	Date finished (2017)	Time finished (h UTC)	Time on hole (days)
U1512A	34°01.6406′S	127°57.7605′E	0	0	0	73	6 Oct	2130	14 Oct	1455	7.73
U1513A	33°47.6084′S	112°29.1338′E	8	7	35	0	18 Oct	0645	23 Oct	0410	4.89
U1513B	33°47.6087′S	112°29.1471′E	8	6	0	0	23 Oct	0410	23 Oct	2225	0.76
U1513C	33°47.6190′S	112°29.1468′E	2	0	0	0	23 Oct	2225	24 Oct	0845	0.43
U1513D	33°47.6196′S	112°29.1339′E	0	0	0	74	24 Oct	0845	1 Nov	1730	8.36
U1513E	33°47.6190′S	112°29.1204′E	0	0	0	7	19 Nov	1910	24 Nov	2125	5.09
U1514A	33°7.2327′S	113°5.4672′E	19	5	7	0	2 Nov	0000	4 Nov	1215	2.51
U1514B	33°7.2335′S	113°5.4798′E	2	0	0	0	4 Nov	1215	5 Nov	0130	0.55
U1514C	33°7.2443′S	113°5.4799′E	0	0	0	34	5 Nov	0130	9 Nov	0935	4.34
U1515A	33°16.1890′S	114°19.3666′E	0	0	0	55	9 Nov	1600	13 Nov	0550	3.58
U1516A	34°20.9169′S	112°47.9553′E	20	9	0	0	13 Nov	1748	15 Nov	0925	1.65
U1516B	34°20.9175′S	112°47.9684′E	2	0	0	0	15 Nov	0925	15 Nov	1945	0.43
U1516C	34°20.9272′S	112°47.9711′E	0	0	0	40	15 Nov	1945	18 Nov	1150	2.67
U1516D	34°20.9277′S	112°47.9573′E	0	0	0	4	18 Nov	1150	19 Nov	1455	1.13
		Totals:	61	27	42	287					

Table T2. Live interactive broadcasts between the ship and shore, Expedition 369. (Continued on next page.)

Date (2017)	Time (h UTC)	Location (state or country broadcasting to)	Organization/School name	Age level	Number of attendees
4 Oct	0100	Washington DC, USA	Smithsonian Institute (Natural History)	Middle school	3
10 Oct	1930	Brazil	Colegio Rogelma A.F.M. Mello	High school	49
11 Oct	2300	Washington DC, USA	Smithsonian Institute (Natural History)	Middle school	22
12 Oct	1700	Casablanca, Morocco	Lycee Francais Internationale	High school	40
13 Oct	2125	New York, USA	Community Partnership Charter School	Middle school	46
16 Oct	1900	Brazil	Colegio Vila Olympia	Middle school	32
17 Oct	2000	Brazil	Colegio Seice	High school	29
18 Oct	1930	United Kingdom	Carmel College	High school	40
18 Oct	2315	Washington DC, USA	Smithsonian Institute (Natural History)	Middle school	20
19 Oct	1600	France	Lycee Paul Vincensini	High school	27
23 Oct	2100	Brazil	Semana Nacional de Ciência e Tecnologia	High school	12
24 Oct	0100	Brazil	Semana Nacional de Ciência e Tecnologia	Middle school	30
24 Oct	2100	Brazil	Semana Nacional de Ciência e Tecnologia	High school	15
25 Oct	0500	Brazil	Semana Nacional de Ciência e Tecnologia	6–7 years	32
27 Oct	0100	Brazil	Semana Nacional de Ciência e Tecnologia	Middle school	15
27 Oct	2100	Brazil	Semana Nacional de Ciência e Tecnologia	Middle school	24
30 Oct	1840	United Kingdom	Belmont Community School	Middle school	36
1 Nov	1500	South Korea	Chonnam National University	College	25
2 Nov	0400	Louisiana, USA	University of Louisiana at Lafayette	Post grad	30
2 Nov	0845	California, USA	Cerritos College	College	25
2 Nov	2140	United Kingdom	Belmont Community School	Middle school	36
7 Nov	2040	Germany	St. Angela School	High school	48
7 Nov	2345	New York, USA	Intrepid Sea, Air, and Space Museum	Teachers/Adults	70
8 Nov	0230	Brazil	IODP meeting	Academics	110
8 Nov	1430	China	Jiayuguan Primary School	Elementary school	45

Table T2 (continued).

Date (2017)	Time (h UTC)	Location (state or country broadcasting to)	Organization/School name	Age level	Number of attendees
9 Nov	0500	Brazil	Colegio Seice	High school	40
9 Nov	2145	Florida, USA	River Ridge High School	High school	60
10 Nov	0150	Missouri, USA	Claymont Elementary School	Elementary school	20
12 Nov	0030	United Kingdom	University of Oxford	College	40
12 Nov	1300	Japan	Japanese Young Scientists School	College	25
13 Nov	1530	Japan	Kanazawa University	College	70
14 Nov	0230	Nebraska, USA	Shickley Public School	Middle school	25
14 Nov	1830	China	Nanjing University	College	40
15 Nov	0100	Michigan, USA	Canton High School	High school	30
16 Nov	0030	Michigan, USA	Canton High School	High school	30
16 Nov	0300	Michigan, USA	Canton High School	High school	30
16 Nov	1530	Germany	Herbartgymnasium	High school	18
17 Nov	0215	Washington D.C., USA	Smithsonian Institute (Natural History)	Middle school	40
17 Nov	2300	United Kingdom	Natural History Museum in London	General public	40
20 Nov	1800	France	Lycee le Likes LaSalle Quimper	High school	30
20 Nov	2030	Texas, USA	Valley View Junior High	Middle school	30
21 Nov	1600	France	Lycee Valin	High school	25
22 Nov	0100	Brazil	Unisinos	College	30
23 Nov	0145	California, USA	Cerritos College	College	30

Table T3. Social media activity during Expedition 369. Numbers as of 1400 h, 23 November 2017. NA = not applicable.

Platform	Number of posts	Number of likes	Number of shares	Number of comments
Facebook	52	3245	424	108
Twitter	89	1100	552	19
Instagram	57	3059	NA	39
Blog	27	NA	NA	NA

Figure F1. Late Cenomanian (94 Ma) and middle Eocene (40 Ma) paleogeographic reconstructions after Hay et al. (1999) showing the location of Expedition 369 sites in the Mentelle Basin (MB; adjacent to Naturaliste Plateau), the Great Australian Bight (GAB), and selected deep-sea sites (DSDP sites 327, 511; ODP sites 689, 690) at southern high latitudes.

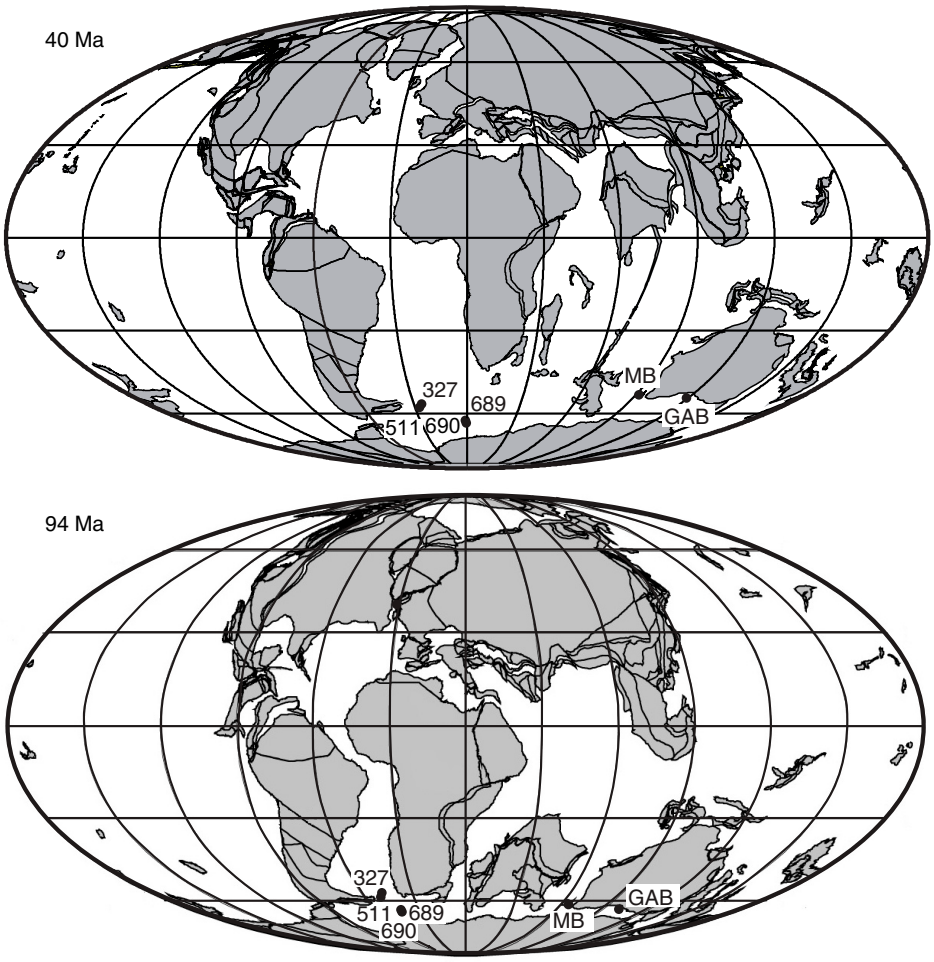

Figure F2. A. Regional context of the NP and MB, including location of the major reflection seismic profiles, DSDP sites, and Expedition 369 sites. PB = Perth Basin, LB = Leeuwin Block, YS = Yallingup shelf. B. Locations of Site U1512 (red triangle) in the GAB, Leg 182 sites, and petroleum exploration wells (black circles).

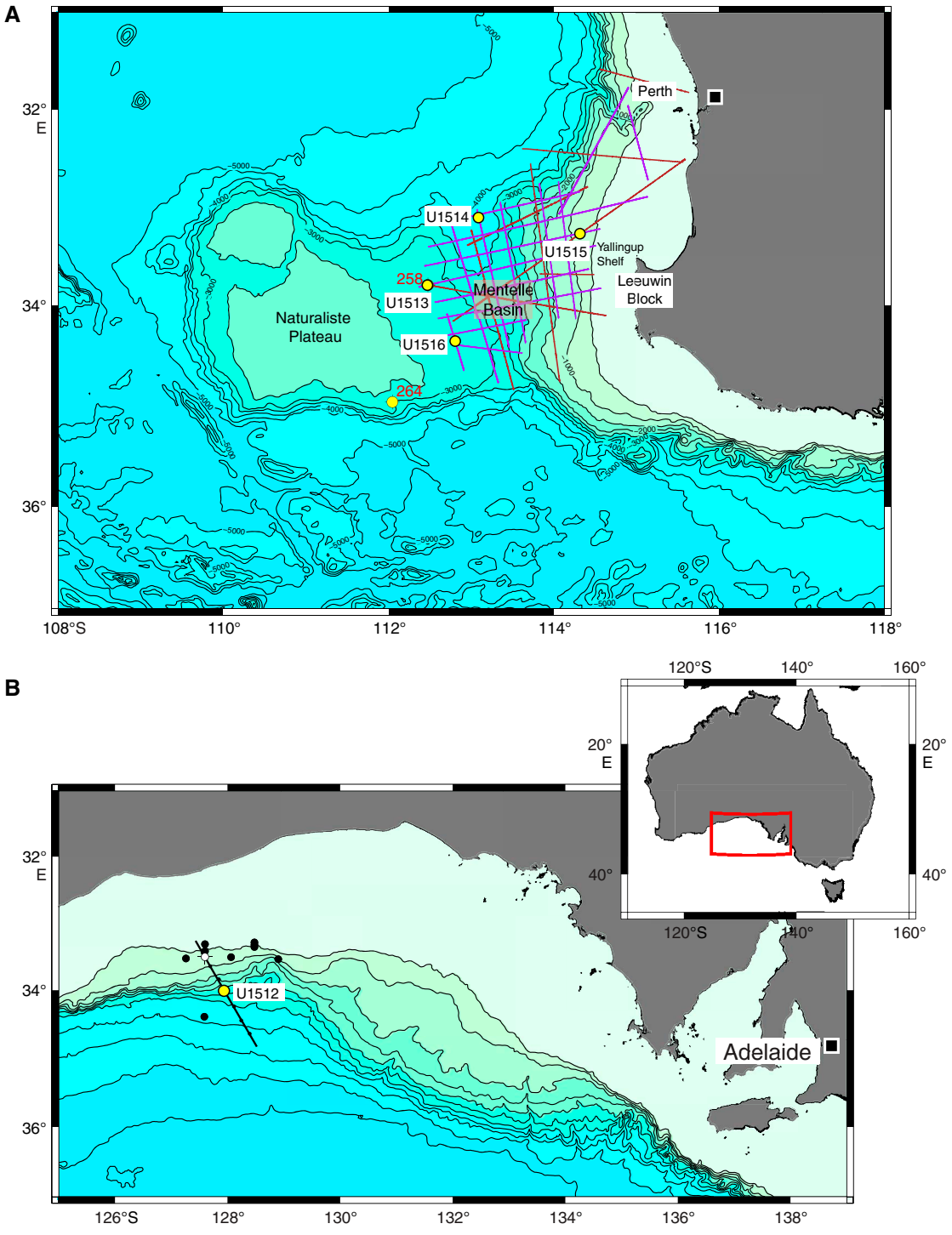

Figure F3. Ocean currents in the modern ocean surrounding Australia. Orage = surface currents, green = intermediate currents, and blue = deep-ocean currents. Yellow circles = Expedition 369 sites.

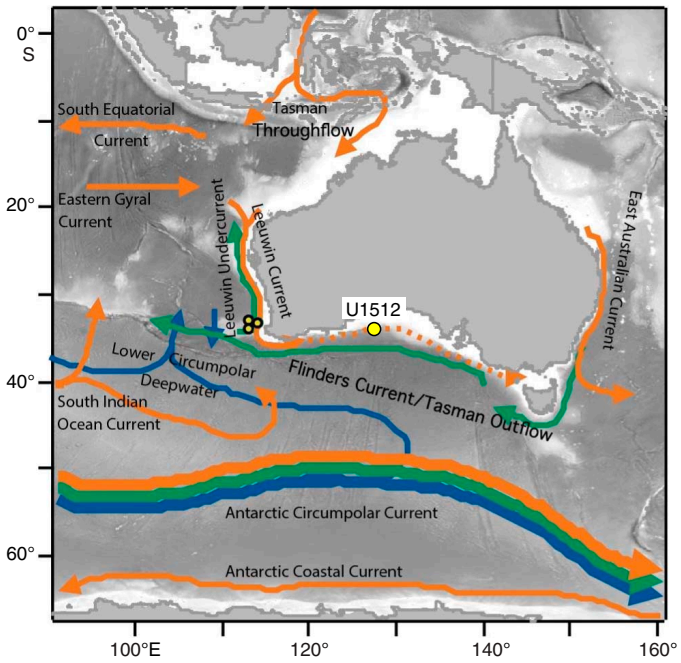

Figure F4. Site U1512 summary. Yellow shading = floating spliced intervals.

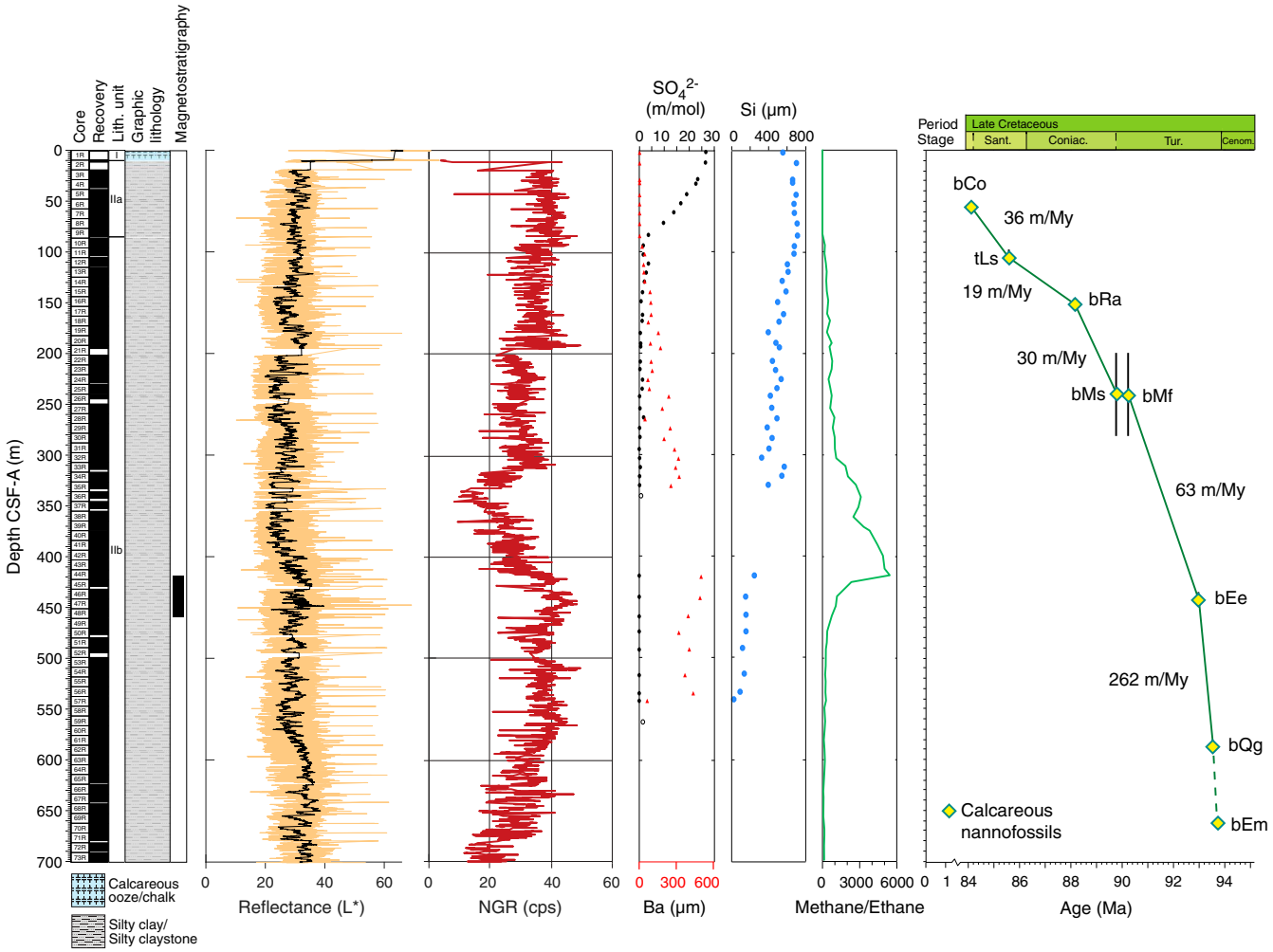

Figure F5. Site U1513 summary. Yellow shading = floating spliced intervals. NGR and core recovery: green = Hole U1513A, light blue = Hole U1513B, dark blue = Hole U1513D. Green (RGB): values outside a 50-point moving average ±1σ were removed and a 50-point moving average was plotted over the data series. Hole U1513C (~17 m) was sampled completely on the catwalk.

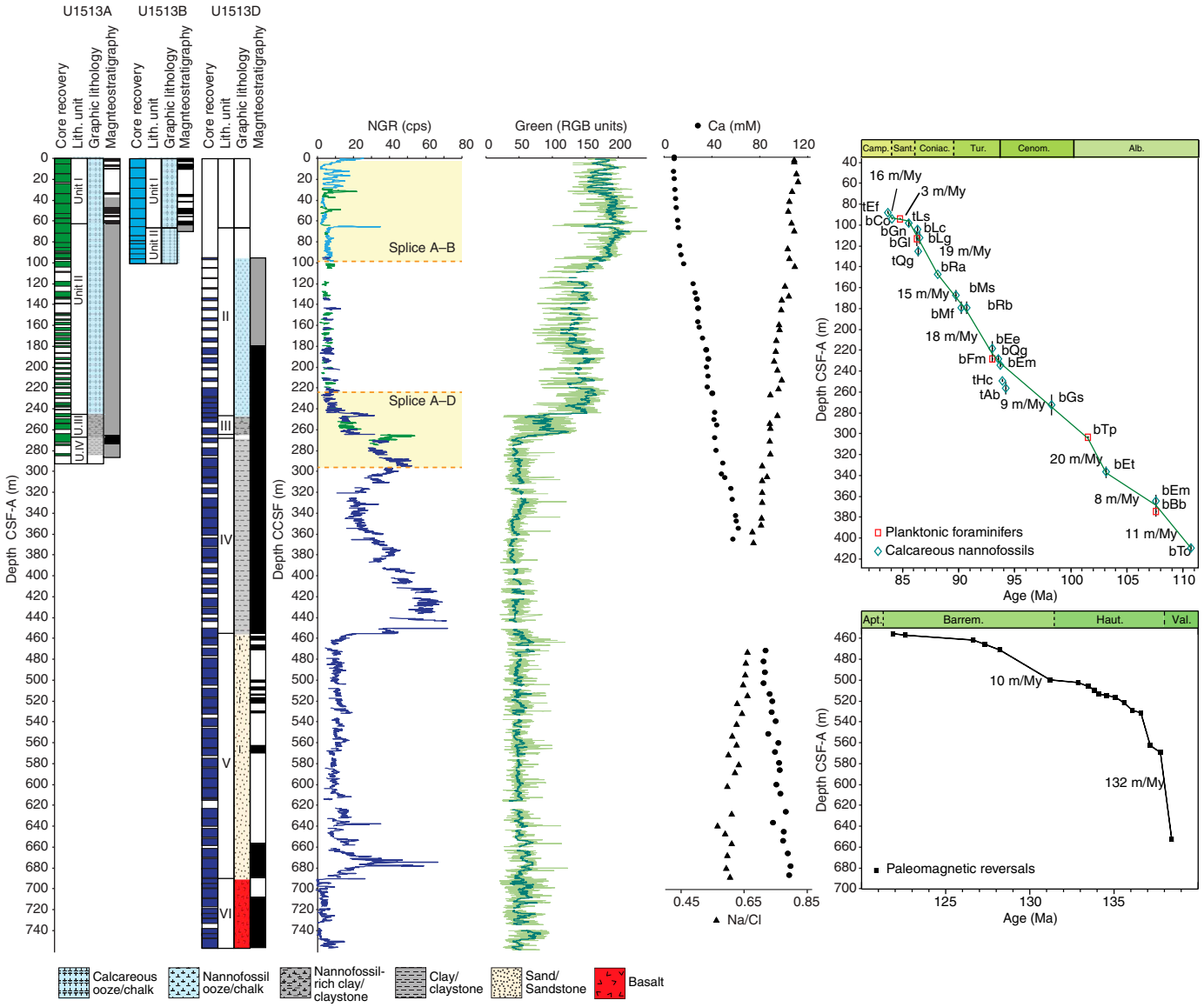

Figure F6. Site U1514 summary. Yellow shading = floating spliced intervals. Core recovery and data: light blue = Hole U1514A, green = Hole U1514C. Hole U1514B (~15 m) was sampled completely on the catwalk.

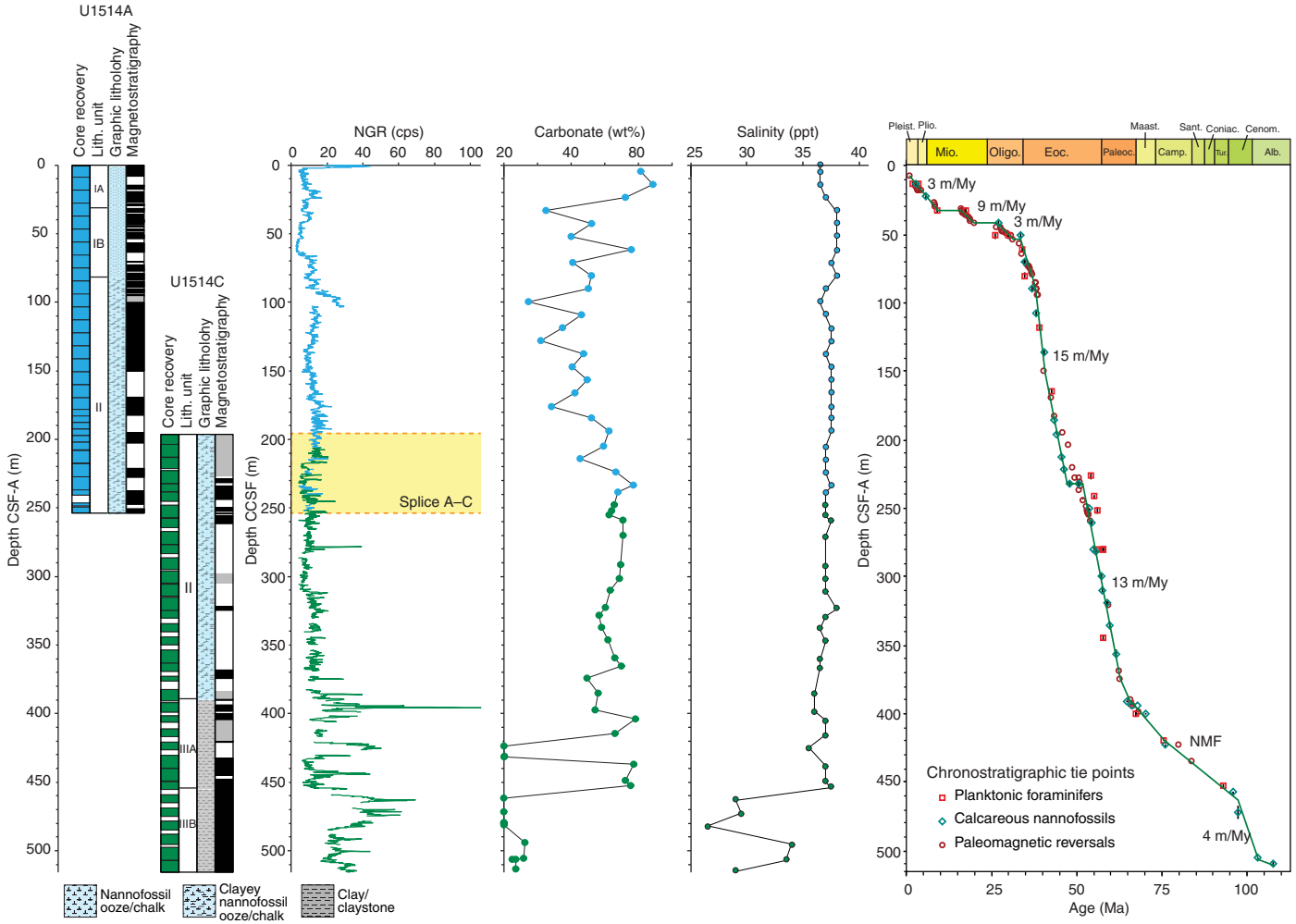

Figure F7. Site U1515 summary.

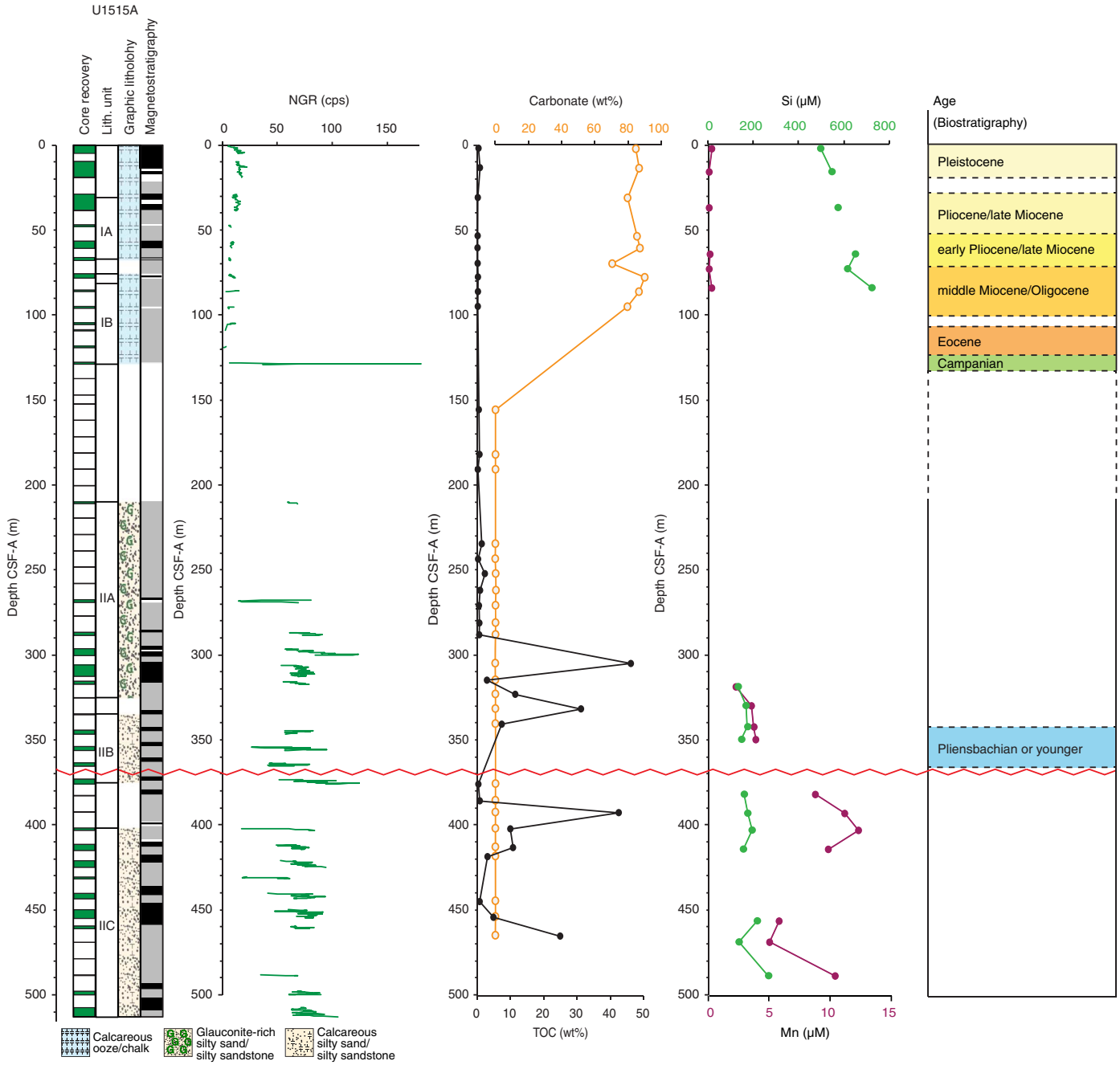

Figure F8. Site U1516 summary. Yellow shading = floating spliced intervals. Core recovery and data: light blue = Hole U15146A, green = Hole U1516C. Hole U1516B (~16 m) was sampled completely on the catwalk.

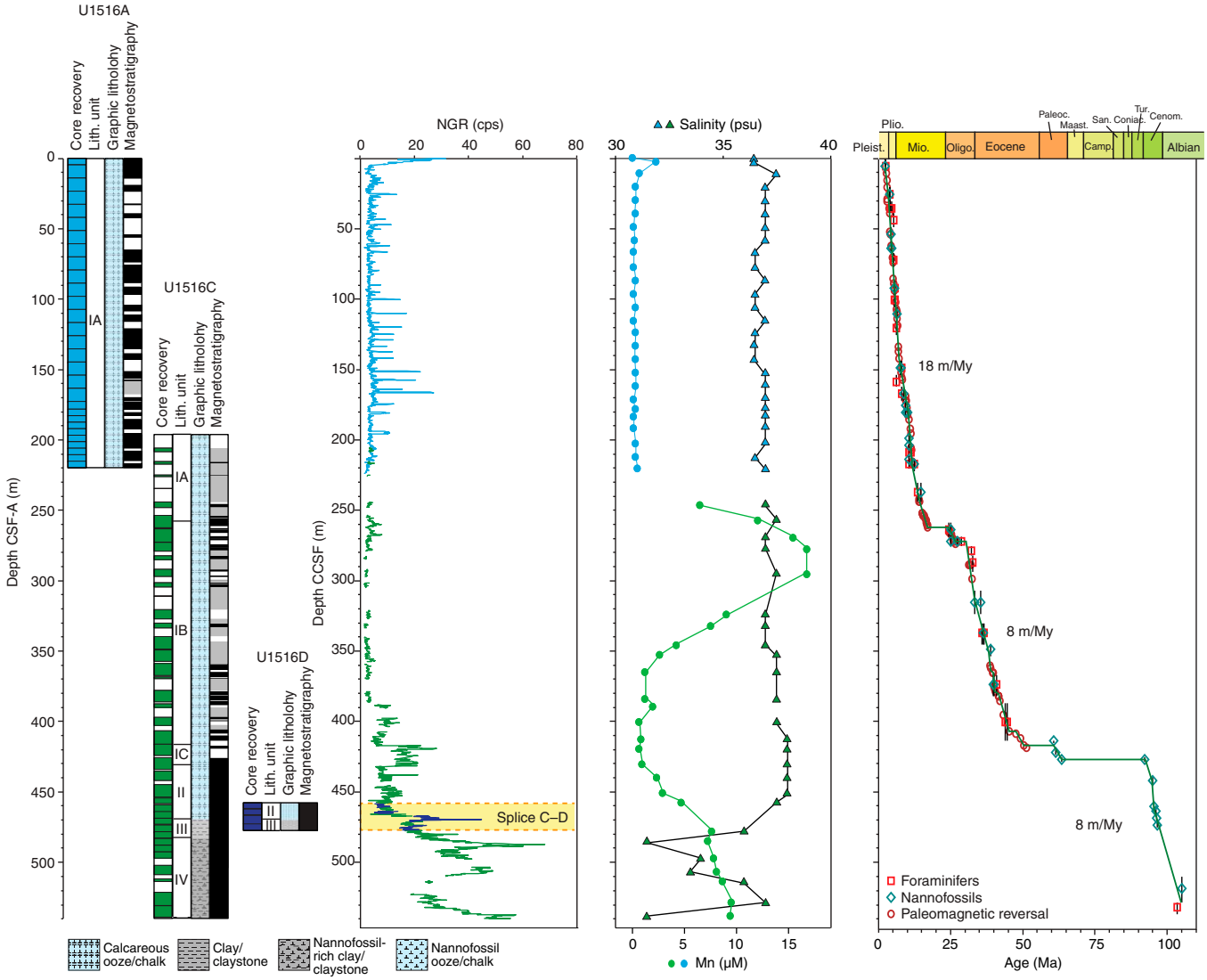

Figure F9. Age-depth plots, Sites U1512–U1514 and U1516. Horizontal lines = unconformities.

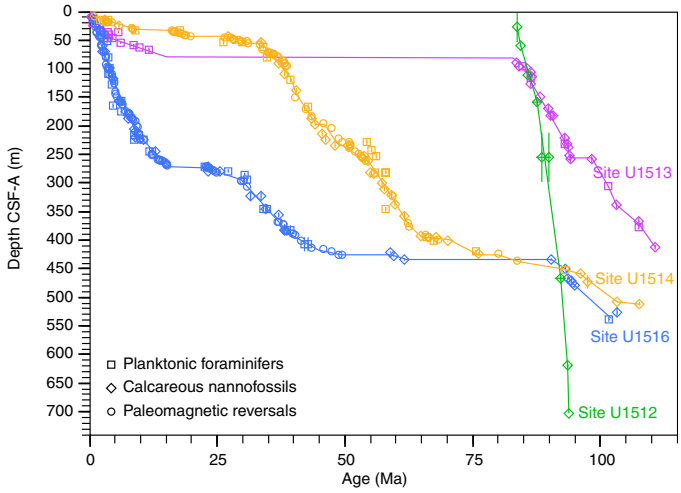

Figure F10. Stratigraphic summary and correlation of NGR records, Sites U1512–U1516 (from west to east). Yellow stars = critical intervals that will be the focus of intensive shore-based study. (This figure is also available in an **oversized format**.)

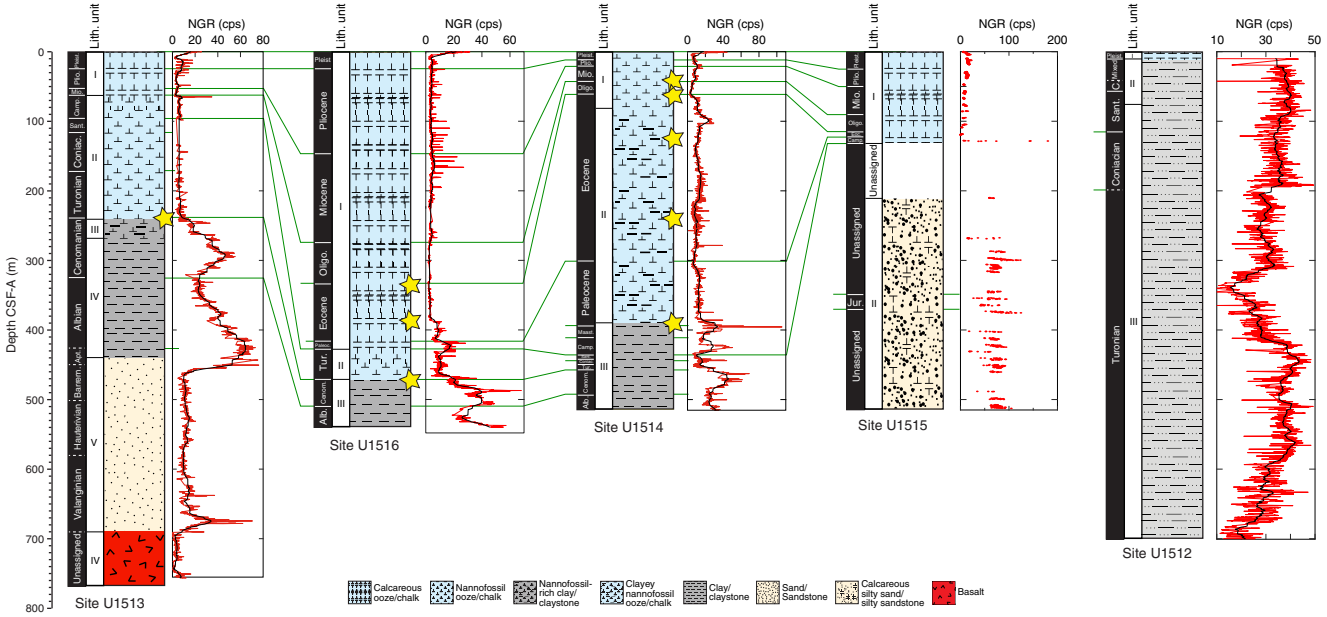

Figure F11. Bulk sediment, geochemical summary, Sites U1512–1516 (west to east).

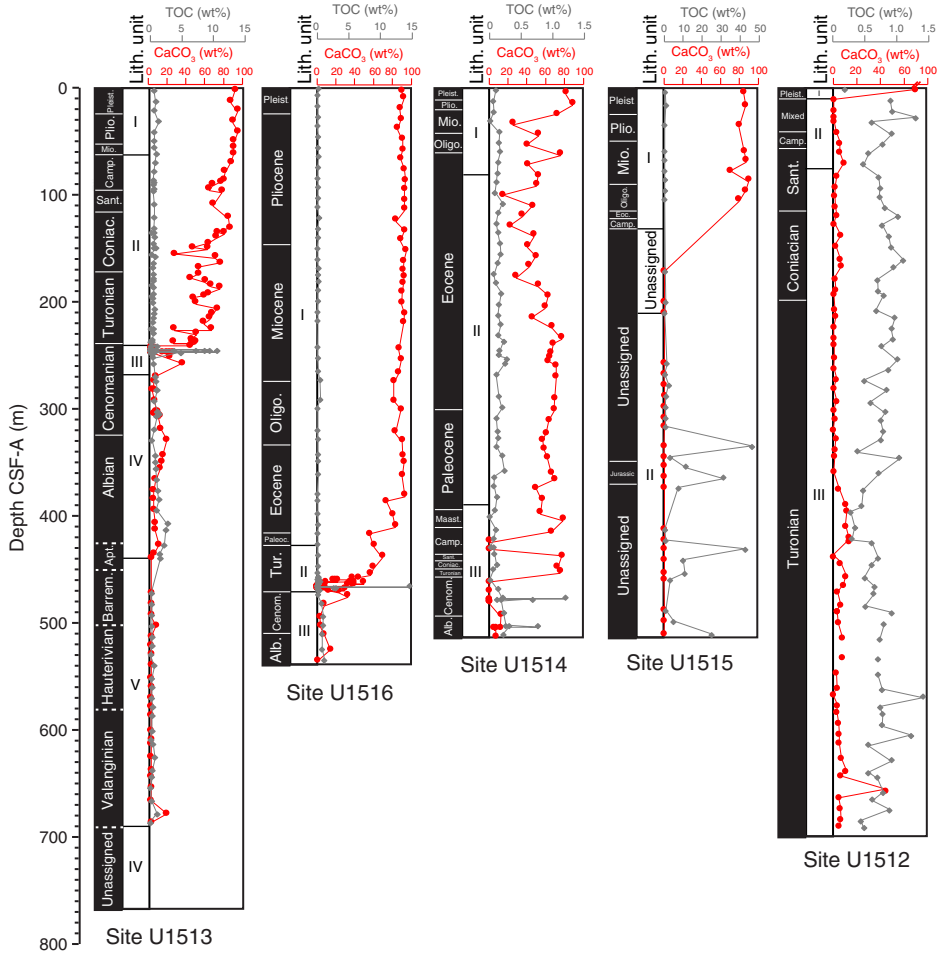

Figure F12. Interstitial water geochemical summary, Sites U1512–U1516 (west to east).